

PAPER

Test of electrical resistivity and current diffusion modelling on MAST and JET

To cite this article: D.L. Keeling *et al* 2018 *Nucl. Fusion* **58** 016028

View the [article online](#) for updates and enhancements.

Related content

- [Overview of recent physics results from MAST](#)
A. Kirk, J. Adamek, R.J. Akers *et al.*
- [TRANSP-evolved q-profiles](#)
D J Kelliher, N C Hawkes, P J Mc Carthy *et al.*
- [Chapter 6: Steady state operation](#)
C. Gormezano, A.C.C. Sips, T.C. Luce *et al.*

Test of electrical resistivity and current diffusion modelling on MAST and JET

D.L. Keeling¹, C.D. Challis¹, I. Jenkins¹, N.C. Hawkes¹, I. Lupelli¹,
C. Michael², M.F.M. de Bock³, the MAST Team¹ and JET contributors^a

¹ Culham Centre for Fusion Energy, Culham Science Centre, Abingdon OX14 3DB, United Kingdom

² The Australian National University, Canberra, Acton ACT 2601, Australia

³ ITER Organization, Route de Vinon sur Verdon, CS 90 046, 13067 Saint Paul Lez Durance, France

E-mail: David.Keeling@ukaea.uk

Received 23 June 2017, revised 17 October 2017

Accepted for publication 19 October 2017

Published 16 November 2017



Abstract

Experiments have been carried out on the MAST and JET tokamaks intended to compare the electrical resistivity of the plasma with theoretical formulations. The tests consist of obtaining motional stark effect (MSE) measurements in MHD-free plasmas during plasma current ramp-up (JET and MAST), ramp-down (MAST) and in stationary state (JET and MAST). Simulations of these plasmas are then performed in which the current profile evolution is calculated according to the poloidal field diffusion equation (PFDE) with classical or neoclassical resistivity. Synthetic MSE data are produced in the simulations for direct comparison with the experimental data. It is found that the toroidal current profile evolution modelled using neoclassical resistivity did not match the experimental observations on either device during current ramp-up or ramp-down as concluded from comparison of experimental and synthetic MSE profiles. In these phases, use of neoclassical resistivity in the modelling systematically overestimates the rate of current profile evolution. During the stationary state however, the modelled toroidal current profile matched experimental observations to a high degree of accuracy on both devices using neoclassical resistivity. Whilst no solution to the mismatch in the dynamic phases of the plasma is proposed, it is suggested that some physical process other than MHD which is not captured by the simple diffusive model of current profile evolution is responsible.

Keywords: plasma resistivity, stationary-state plasmas, classical, neoclassical resistivity, diffusion

(Some figures may appear in colour only in the online journal)

1. Introduction

The experimental investigation of the electrical resistivity of tokamak plasmas has been an ongoing area of research amongst the worldwide community since the publication of the classical formulation of plasma resistivity by Spitzer and Härm [1]. This formulation was later extended to correct the classical expression for the effects of a poloidally non-uniform magnetic field strength in an axisymmetric toroidal plasma, resulting in the neoclassical theory of resistivity [2]. In earlier experiments, before the early 1990s [3], profile

measurements of toroidal current (I_p) density were unavailable and comparisons of experiment with theory to assess resistivity were based on global rather than profile measurements. Ohm's law was used to compare calculations of resistivity with measured loop voltage or to calculate a value of the effective average ion charge (Z_{eff}) where a direct measurement of this quantity was unavailable. Such experiments showed, in the PLT device, inconsistency of calculated resistivity with neoclassical theory [4] and consistency with Spitzer resistivity [5] whilst the inconsistency with neoclassical theory was also shown in the Doublet III device [6]. ASDEX produced contradictory results finding consistency with Spitzer resistivity in one experiment [7] and with neoclassical in another [8]. The

^a See the author list of X. Litaudon *et al* 2017 *Nucl. Fusion* 57 102001.

FTU team also reported that resistivity appeared to be closer to Spitzer than neoclassical [9] whilst in Alcator-C-Mod the resistivity was found to lie in between that predicted by neoclassical and Spitzer [10]. In contrast, experiments on JIPP T-II [11], JET [12, 13], JT-60 [14], TFTR [15], and Tore-Supra [16] found the resistivity to be in agreement with neoclassical theory.

Developments in diagnostic capability including measurements based on Li beam [17] or motional stark effect (MSE) [18] enabled profile measurements of toroidal current density allowing more detailed tests of plasma resistivity to be made. Using these techniques, on ASDEX [19], TEXT [20], and PBX-M [21] the resistivity was found to be closer to classical Spitzer although it is noted that deviations from both Spitzer and neoclassical models were seen. In the conclusion of the review by Kikuchi and Azumi [3], it is noted that the larger devices JT-60, TFTR and JET show good agreement with neoclassical theory, also confirming the existence of the neoclassical bootstrap current, but the I_p profile measurements from the smaller devices ASDEX, TEXT and PBX-M require further investigation to understand the disagreement with neoclassical theory.

Since the publication of the review summarized above [3], further experiments have taken place benefitting from the more widespread use of diagnostics such as MSE and far-infrared polarimetry [18, 22] allowing more precise determination of the I_p profile. Experiments in TEXT-Upgrade [23] showed agreement with Spitzer resistivity in a sawtooth plasma whilst experiments in DIII-D [24] showed agreement with neoclassical theory in a neutral-beam heated plasma discharge dominated by inductively driven current immediately following the plasma I_p ramp-up phase. An investigation by Batha *et al* [25] in TFTR comprised tests specifically carried out during perturbations to I_p , in both ramp-up and ramp-down phases. It was found that neither neoclassical nor Spitzer resistivity models correctly predicted the evolution of the poloidal field during these phases. Neoclassical theory generally gave a prediction that was closer to the experimental value than Spitzer in the outer half of the plasma (though still differing from the experimental result by up to 2 standard deviations) and both models gave inaccurate predictions in the plasma core. In contrast to this result, modelling of plasmas typically featuring internal transport barriers (ITBs) on JET [26], starting in the latter half of the I_p ramp but after initial pre-heating, showed neoclassical resistivity gave a good description of the current profile evolution throughout the final stage of the I_p ramp and into the main heating phase.

The production of the Improved H-mode (also known as ‘hybrid mode’) on ASDEX Upgrade [27], in which the value of the safety-factor (q) remains at or just above 1 in the centre out to $r/a \sim 0.4$ – 0.5 , has presented a further challenge to current diffusion modelling. Initially, it was suspected that core-localised MHD such as fishbones in ASDEX Upgrade [27], NTMs in the case of DIII-D [28] or an internal 1/1 kink-mode on JT-60U [29], was responsible for the form of the q -profile and that a current diffusion simulation could not be expected to reproduce the experimental observations. In simulations of the DIII-D hybrid mode, a spatially localized

hyper-resistive term was included in Ohm’s law with neoclassical resistivity which allowed current diffusion simulations to reproduce the experimental observations [30] whereas in JT-60U an enhanced neoclassical resistivity scheme was proposed [31]. Later studies on ASDEX Upgrade demonstrated that the hybrid mode could be sustained in MHD-free conditions for several seconds [32] and in which current diffusion codes still failed to correctly reproduce the observed I_p profile using either Spitzer or neoclassical theory. Instead, the modelled current penetration was markedly more rapid than experimental measurements suggested, a phenomenon also observed on JET [33] during the early phase of the I_p ramp-up and MAST [34] in the latter half of the I_p ramp-up in conditions of no or negligible MHD, and in ASDEX Upgrade [35] during early I_p ramp-up. In the latter case, it was again argued the presence of fishbones or NTMs was responsible for current redistribution and the observed disagreement between modelling and experiment. Agreement with modelling was obtained on JET [36] using a technique to tune certain plasma parameters within their experimental error to achieve a match of the time at which q_0 reached a value of ~ 0.7 with the time of the first observed sawtooth crash. In this case, the simulations were performed with neoclassical resistivity and agreement between simulation and experiment was shown. In further studies on JET investigating the effect of auxiliary current drive (CD) on advanced scenarios [37], modelling with neoclassical resistivity was reported to give a very good agreement between measured and simulated loop voltage in plasmas with RF-CD. In these experiments however, the simulated q -profile showed some deviation from that inferred from MSE-constrained EFIT [38] despite the good match with loop-voltage, whilst the discrepancy between simulation and observation remained in experiments looking specifically at lower-hybrid CD [39]. A further investigation of the I_p flat-top phase in JET hybrid mode plasmas found good agreement between MSE data and modelling [40].

From consideration of these varied findings it is clear that there are a number of open questions regarding plasma resistivity in tokamaks. Although, generally, larger hotter devices appear to follow neoclassical resistivity in near stationary-state, there are still some unexplained instances where this is not the case. In contrast, many smaller devices appear to lean more towards Spitzer resistivity though there are documented cases where neoclassical is the better description. In I_p ramp experiments, there are likewise cases that appear to agree with neoclassical theory and also cases where this is not a good description. The hybrid-mode of operation adds to the list of case-studies in that it is not well explained by either neoclassical or Spitzer resistivity but rather that the total resistivity is larger than either of these theories predicts. In this mode of operation in ASDEX Upgrade and JET for example, MHD such as $n = 1$ fishbones are often excited and may be accounted for in subsequent modelling by appropriate modifications to Ohm’s law. However, there are also cases of MHD-free hybrid-mode plasmas where such modification is not applicable.

Furthering understanding of current diffusion in plasmas is therefore an important area of tokamak research in order

to effectively analyse present experiments and improve reliability of predictive capability for future devices such as ITER. This is of particular importance in the I_p ramp-up phase which is typically used for formation of a particular target q -profile with desired properties for the plasma scenario under investigation. For example, monotonic q -profiles are typical of the JET baseline plasma scenario [41], whilst q -profiles in the hybrid mode, although still monotonic, are flatter in the plasma core region [42]. The latter relies on appropriate modification of the current diffusion within the first few seconds of the plasma discharge to arrive at the correct q -profile at the time the main heating power is applied.

In this paper, analysis of experiments carried out on the JET and MAST tokamaks is presented. Together with new results, an extended analysis of carbon-wall JET plasmas reported in [33] and further analysis of MAST plasmas reported in [34] is included. The organisation of this paper is as follows: in section 2 a description of the experiments and interpretive analysis carried out on both devices is presented. Section 2.1 first describes the salient features of the modelling codes used for interpretive analysis of the experiments shown in the rest of section 2. Section 2.2 then deals with experiments on the JET tokamak showing firstly that current diffusion modelled using neoclassical theory disagrees with experimental data in I_p ramp-up but shows good agreement in stationary state. In section 2.3, similar analysis is shown for the MAST tokamak again showing disagreement between modelling and experiment in I_p ramp-up and ramp-down, but good agreement in stationary state. These results contrast with those reviewed in the introduction above by demonstrating periods in the evolution of a plasma where modelling and experiment do not match (dynamic I_p phases), and periods in different plasma discharges on the same device where they do match (stationary-state). Furthermore, it is shown that similar results are obtained from very different machines: JET, a large, conventional aspect ratio device and MAST, a small, tight aspect ratio device. Throughout section 2, the modelling is carried out using the TRANSP analysis code [43]. In order to demonstrate that the mismatch between modelling and experiment shown in section 2 is not due to errors in the calculation of resistivity in the TRANSP code, a comparison with independently calculated resistivity profiles is shown in section 3. A discussion of these results is presented in section 4 with final conclusions.

2. Experiments

2.1. Plasma modelling

Throughout the rest of this article, the principal modelling tool is TRANSP, a time-dependent interpretive code [43]. TRANSP takes a number of time-dependent data traces and profiles as input: the 2D plasma boundary (i.e. the last closed flux surface) usually calculated by EFIT from magnetics data; plasma current and toroidal magnetic field, also from magnetics data; electron temperature and density profiles from Thomson scattering diagnostics; radiation data from bolometry; effective charge data from bremsstrahlung measurements; and fuelling

information based on calculations of gas flow through the gas introduction systems. When neutral beam injection is active, charge-exchange data may also be available providing profiles of ion temperature and bulk toroidal rotation velocity. In the absence of charge-exchange data it is usual to assume $T_i = T_e$ and rotation is zero (both reasonable assumptions in cooler, highly collisional plasma regimes with no externally supplied torque). An internal equilibrium solver (usually the Lawrence Livermore National Laboratory code, TEQ) solves the Grad-Shafranov equation using the supplied data. This then enables solution of the 1.5 D generalized transport and poloidal field equations.

The poloidal field diffusion equation (sometimes referred to as the magnetic diffusion equation in the literature) is derived in [2] where the time evolution of the poloidal flux function ψ with respect to a surface labelled by the constant toroidal flux ϕ is

$$\left. \frac{\partial \psi}{\partial t} \right|_{\phi} = \frac{\langle E_{\parallel} B \rangle}{F \langle R^{-2} \rangle} \quad (1)$$

where $F \equiv RB_T$, R is the major radius and B_T is the toroidal field, $\langle \dots \rangle$ denotes a flux-surface averaged quantity and the parallel electric field E_{\parallel} is expressed as

$$E_{\parallel} = \eta_{\parallel} (J_{\parallel} - J_{\text{ex}}) \quad (2)$$

where η_{\parallel} is the plasma parallel resistivity and J_{\parallel} and J_{ex} are the parallel and externally driven currents respectively. TRANSP uses an arbitrary time-dependent 2D magnetic geometry based on the toroidal flux $\phi(\rho) = \pi \rho^2 B_0$ where ρ is the absolute flux surface label and $\phi_{\text{lim}} = \pi \rho_{\text{lim}}^2 B_0$ is the flux enclosed by the plasma. Differentiating equation (1) with respect to ρ then gives an expression for the time derivative of the effective poloidal magnetic field in terms of the spatial derivative of the effective parallel electric field

$$\frac{\partial B_{\text{po}}}{\partial t} = \frac{\partial E_0}{\partial \rho} \quad (3)$$

where the effective poloidal magnetic field magnitude $B_{\text{po}}(\rho, t)$ is defined as

$$B_{\text{po}}(\rho, t) \equiv \frac{1}{R_0} \frac{\partial \psi}{\partial \rho} \quad (4)$$

and the effective parallel electric field E_0 is

$$E_0 \equiv \frac{\langle E_{\parallel} B \rangle}{FR_0 \langle R^{-2} \rangle}. \quad (5)$$

TRANSP is run in analytic mode, producing a self-consistent equilibrium at each time step from the input data and the current profile (at initialization of the simulation, the current profile is determined from a supplied initial q -profile which is usually obtained from a suitable EFIT equilibrium.) Equation (3) is solved at each time step by TRANSP to evolve the poloidal magnetic field using an expression for the plasma parallel resistivity. Choices for the resistivity used in this paper are either the classical (Spitzer) resistivity [1], or neoclassical resistivity obtained from either the NCLASS code [44] or the Sauter model [45, 46]. There is also the possibility

to constrain the current profile in the simulation such that the simulation matches a supplied q -profile for the full duration of the simulation (e.g. from MSE-constrained EFIT). In this case the output is the inferred plasma resistivity profile.

NCLASS is a multi-fluid model for the parallel and radial force balance equations from which the neoclassical bootstrap current, parallel electrical resistivity, impurity and fuel ion radial particle transport, and plasma poloidal rotation can be determined. This code is valid for arbitrary plasma shape and collisionality through the use of interpolation formulas for viscosity from low to high collisionality regimes. NCLASS has been shown to be a reliable description for JET plasmas in some previous studies [12, 13, 40] so has been used in the present work for JET simulations. Sauter *et al* attempted to address two issues with the NCLASS code: firstly, that of computational expense due to the need to solve a set of equations and secondly the fact that NCLASS does not use a full collision operator which can lead, in certain cases, to errors of up to 20%. Sauter's approach was therefore to use a code to solve the Fokker–Planck equation using a linearized collision operator on flux surfaces from an exact axisymmetric magnetic configuration as calculated by a toroidal equilibrium code. The transport equations were then solved over a wide variety of equilibria, trapped particle fraction and collisionality to determine fitted formulas for neoclassical resistivity and bootstrap current coefficients relative to the pressure, and the electron and ion temperature gradients. In this way, the computational efficiency of the solution of the problem is improved with a better representation of the collision operator but at the expense of the fitted formulas possibly performing poorly in parameter spaces not investigated during the production of the fits.

In the regimes investigated in the present work, both of these formulations are expected to be adequate though the Sauter fits were previously shown to produce marginally better results in determining the loop voltage in stationary-state experiments on MAST. Therefore, NCLASS was generally used for analysis of JET plasmas whilst Sauter was used for MAST [47]. It should be noted that tests of both formulations have been performed for plasmas on both machines with no appreciable difference seen between them other than that mentioned above.

Whilst the NCLASS and Sauter formulations are independent, they have both been implemented in the context of the TRANSP computational environment in the present work. In section 3, a test is carried out to verify that the resistivity profiles calculated by these codes in TRANSP can be reproduced by a formulation of the neoclassical theory independent of the TRANSP environment. For this test the NEO code is used [48]. NEO is a local drift kinetic neoclassical transport model with a complete linearized Fokker–Planck multispecies collision operator. In the plasma regimes analysed in the present work it is shown in section 3 that the results from these codes are very similar despite their various differences.

2.2. JET experiments

Various techniques may be used to control the current diffusion during the early phase of a tokamak discharge such as I_p ramp-rate modification or auxiliary heating and current-drive.

Such techniques, though useful, present a certain challenge to modelling so most of the experiments included in this investigation were designed to test modelling under the simplest possible conditions: L-mode plasma with no auxiliary heating, static plasma shape and in the experiments examining constant I_p ramps, the ramp-rate was kept constant. Experiments from the two tokamaks JET and MAST are presented. Being able to carry out similar experiments on machines with very different size, aspect ratio and toroidal field strength provides an interesting comparison as it allows a test of the theory over a wide range of parameter space in terms of length scale, collisionality and trapped particle fraction which is enhanced on the spherical tokamak compared with conventional aspect ratio.

A plasma with no additional heating has the advantages that no fast-ion (FI) population will be present, eliminating uncertainties due to classical and non-classical FI transport and FI induced MHD and minimising the magnitude of neoclassical bootstrap current. However, the requirement for neutral-beam injection to provide a source for MSE measurements means NBI injection at some point is necessary. To obtain MSE measurements during an ohmic-heating phase, it is necessary to ensure that any neutral beam injection is as non-perturbative as possible such that the measurement still accurately represents the evolution of the plasma with only ohmic-heating.

2.2.1. Re-analysis of I_p ramp experiment. A typical JET plasma has a very rapid current rise phase immediately after breakdown to about 400 kA toroidal current. During this phase the plasma is expanded to a volume which is then generally kept static for the rest of the I_p ramp to flat-top. The rest of the I_p ramp then proceeds at a pre-programmed current rise rate of about 0.2–0.4 MA s⁻¹ until the flat-top level is reached (in the range 1.0–3.5 MA) several seconds after breakdown. For the current-ramp experiment performed for the study in [33], the current ramp rate was approximately 0.4 MA s⁻¹, this being typical of a hybrid-mode plasma.

To provide an experimental measurement of the q -profile, it is necessary to fire a single neutral beam to provide the source for MSE measurements. Due to the very low density levels early in the I_p ramp, there is a limitation on the duration for which the NBI can be applied: 0.5 s, in order to prevent any damage to the torus inner wall from excessive shine-through heat loading. The timing of the measurement was chosen to be as early in the discharge as possible to test the most extreme conditions of the current ramp whilst the plasma is at low temperatures and the current diffusion should be fastest. In the plasma scenario used in this investigation, executed during the final carbon-wall campaign before installation of the Iiter-like wall, the plasma shape transitioned to a diverted configuration soon after the initial rapid current rise phase at $t = 41.3$ s and maintained the same shape for the rest of the current ramp. The MSE measurements were taken immediately after the transition to the diverted configuration in the period 41.4 to 41.9 s. Time-traces of the principal plasma parameters are shown in figure 1 including the NBI power defining the period for the interpretive simulations.

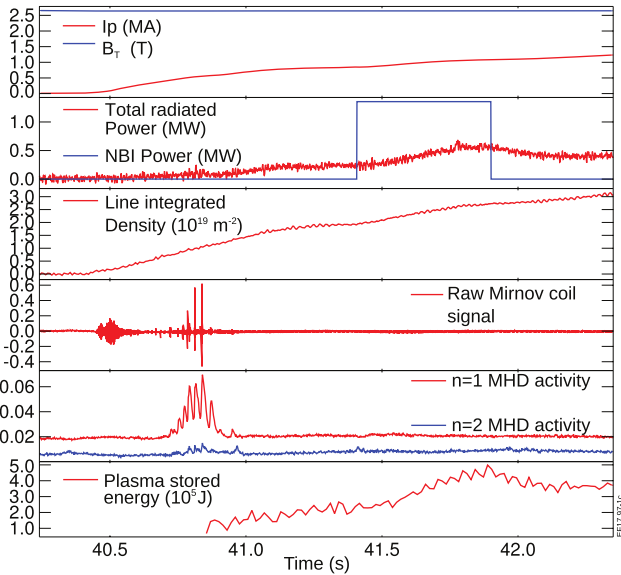


Figure 1. Time traces of principal plasma parameters for JET pulse 79649. Simulations are carried out during the 400 ms NBI phase 41.5–41.9 s which is seen to be free from any significant MHD activity. (N.B. some images in colour in online version only.)

As discussed previously and shown in figure 1 the plasma scenario is kept as simple as possible: a moderate I_p ramp rate of 0.38 MA s^{-1} , 2.6 T toroidal field which reaches a steady value before the plasma breakdown and no auxiliary heating or current drive was applied. The plasma shape was maintained as static as possible to remove any effects potentially introduced by plasma shaping changes. Similarly, the plasma density was ramped up steadily with no large discontinuities, which again simplifies the case for modelling without strong effects from e.g. sudden large influxes of neutrals which could produce sudden cooling of the plasma edge. During the time of interest, the fast-ion (FI) population from the single neutral beam required for MSE measurements represents approximately half of the total plasma pressure in the plasma core (as calculated by TRANSP/NUBEAM) with the ratio $P_{\text{FI}}/P_{\text{therm}}$ falling approximately linearly with radius to ~ 0 at the plasma edge. For this equilibrium, this fast-ion pressure is insufficient to drive any MHD that may affect the result, as seen from the raw Mirnov coil signal and from the processed MHD activity monitors for $n = 1$ and $n = 2$ modes, which show no activity in the period during which the NBI was switched on. The effect on the plasma of this beam can therefore be considered largely non-perturbative from the point of view of current diffusion modelling (i.e. minimal plasma heating and non-inductive current drive, no FI-induced MHD), although the fast-particle population is fully accounted for in the simulations.

Interpretive simulations of the current ramp phase were subsequently carried out with the TRANSP code. Electron temperature and density profiles were provided by a high-resolution Thomson Scattering system, Z_{eff} was determined from visible Bremsstrahlung measurements and ion temperature was assumed equal to electron temperature whilst the plasma boundary was determined from EFIT constrained by magnetics measurements. It is noted that the Z_{eff} value is a time-dependent plasma average rather than a profile so can

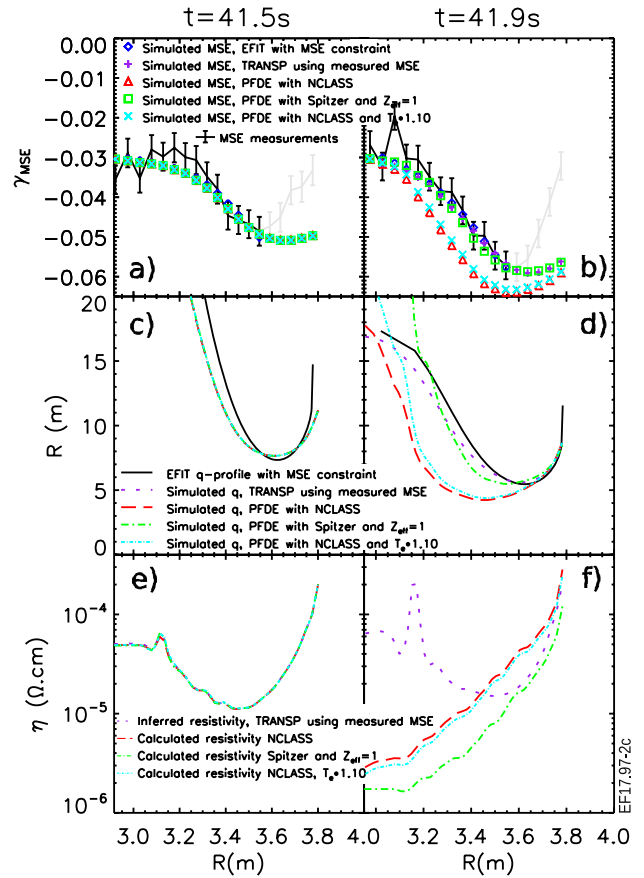


Figure 2. Radial profiles of measured and synthetic MSE data, q -profiles and resistivity profiles at the start and end of the TRANSP simulation for JET pulse 79649. (a) MSE measurements with error bars at the start of the simulation period, 41.5 s, with simulated MSE data from: EFIT with MSE constraints (blue diamonds); TRANSP with q -profile required to match EFIT MSE constrained q -profile (purple crosses); TRANSP with q -profile evolved by poloidal field diffusion equation (PFDE) using NCLASS neoclassical resistivity (red triangles); TRANSP with q -profile evolved by PFDE using Spitzer classical resistivity and $Z_{\text{eff}} = 1$ (green squares); TRANSP with q -profile evolved by PFDE using NCLASS neoclassical resistivity and $T_e \times 1.10$ (cyan crosses). (b) MSE data, as described for panel (a), at the end of the simulation run time: 41.9 s. (c) q -profiles from the various EFIT and TRANSP simulations described above at the start of the simulation. (d) q -profiles from the various EFIT and TRANSP simulations at the end of the simulation. (e) Resistivity profiles from the TRANSP runs at the start of the simulation. (f) Resistivity profiles from the TRANSP runs at the end of the simulation.

be considered a possible source of error in the modelling. The sensitivity of the modelling to this parameter is discussed further later in this section. An important quantity in these simulations is the assumed initial condition for the q -profile. In the experiments described, the initial condition is taken from EFIT constrained by the MSE measurements along with magnetic and kinetic data for $t = 41.5$ s, i.e. as soon as the neutral beam switches on. Thus, the initial condition can be considered a realistic representation and is detailed in figures 2(a), (c) and (e). In figure 2(a), the MSE measurements are shown together with their experimental errors. The MSE diagnostic measures the internal magnetic-field pitch angle $\gamma(r) = \tan^{-1} [B_p(r)/B_T(r)]$ where B_T is the toroidal magnetic

field and B_p is the poloidal field [18]. In figure 2 and other figures later in this article, the pitch angle measurements are shown from a number of lines-of-sight through the plasma. Points with line-of-sight tangency radii $R > 3.55$ m have been flagged as ‘invalid’ data by the MSE post-processing software for reasons such as excessive signal contamination from other sources of light. EFIT uses the valid MSE data as one of the input constraints (along with other constraints such as magnetic and kinetic pressure profiles) and outputs the equivalent MSE signal once the equilibrium solution has converged to within set tolerances, these points are shown as blue diamond markers in figure 2(a). These points are clearly a good match at most radii with a small discrepancy for radii in the range $3.1 \text{ m} < R < 3.3 \text{ m}$. The MSE pitch angle is related to the safety factor, in the cylindrical limit, $q(r) = r/R \tan[\gamma(r)]$. The q -profile resulting from the MSE-constrained EFIT, used as the initial condition for the TRANSP poloidal field diffusion (PFD) calculation, is shown in figure 2(c).

The synthetic MSE data was also obtained from the TRANSP simulations which allow direct comparison with the measurement. The specification of the MSE diagnostic is via a set of geometrical coefficients for each line-of-sight of the diagnostic with respect to the injection geometry of the neutral beam. The TRANSP simulation was carried out three times with different settings to investigate the effects on the calculation of current diffusion. In the initial simulation, the current diffusion is not calculated, the plasma current profile is constrained to match the supplied q -profile determined from MSE-constrained EFIT. This simulation is executed to benchmark the synthetic MSE diagnostic in TRANSP against the equivalent synthetic signal in EFIT. In figure 2(a), this output is shown by purple crosses and, as expected, is seen to match the EFIT simulated MSE points with a high degree of precision. The good match between the simulated MSE points lends confidence that this q -profile represents a good initial condition. Similarly, at the end of the simulation period, the synthetic MSE data from this TRANSP simulation is still seen to match both the experimental data and the MSE constrained EFIT, as detailed in figure 2(b).

The other two TRANSP simulations represent different assumptions for resistivity. The first of these was executed assuming neo-classical resistivity calculated by NCLASS [44]. Further simulations then aim to demonstrate the effect of changing the principal factors that determine the plasma resistivity. Although the precise details of the calculated resistivity are contained within the NCLASS and Sauter models, the trends of the value of the resistivity with certain plasma quantities are believed to still be approximately represented by the classical formulation due to Spitzer and Härm [1] which can be modified with geometrical factors to give a reasonable estimate of neoclassical resistivity. In Spitzer’s formulation, the classical resistivity for singly charged ions is given by

$$\eta_s = 0.51 \frac{m_e^{1/2} e^2 \ln \Lambda}{3 \varepsilon_0^2 (2\pi T_e)^{3/2}}.$$

In which m_e is electron mass, e the electron charge, $\ln \Lambda$ the coulomb logarithm, ε_0 the vacuum permittivity and T_e the

electron temperature. To account for plasmas containing ions with higher Z , a reasonable approximation is that the resistivity is proportional to the effective charge of the plasma ions, Z_{eff} . Furthermore, to a first approximation, the neoclassical correction required to account for the trapped particle fraction can be calculated from consideration of the plasma inverse aspect ratio: $\frac{r}{R}$. If it is assumed that this ratio does not vary significantly between experiments on a particular machine then it can be stated that resistivity is principally affected by changes in electron temperature and in the plasma effective charge. In order to change the rate of current penetration in the model in the appropriate way to achieve a better match to experiment, the resistivity needs to be decreased which implies a decrease in Z_{eff} or an increase of T_e . Another factor that can reduce the effective resistivity is to neglect the neoclassical corrections and simply use Spitzer’s classical formula directly. Combinations of these effects have been tested and two such instances are shown to illustrate the difference these changes make to the simulations. Firstly, a possible systematic error in T_e measurement is tested by increasing the temperature in the simulation by 10% (this is the maximum error associated with the Thomson scattering instrument used to obtain the temperature data). Secondly a simulation using Spitzer resistivity with $Z_{\text{eff}} = 1.0$ is shown. Spitzer resistivity is applicable in plasmas in the absence of magnetic fields and contains no correction for trapped particles, it is therefore quite an extreme departure from the expected neoclassical resistivity paradigm. Similarly, setting $Z_{\text{eff}} = 1.0$ effectively tests the maximum possible departure from the measured Z_{eff} that would decrease the resistivity used in the PFD calculation. The combination of these two changes represents the most extreme plausible departure from the expected resistivity to test how extreme an adjustment is necessary to match the current diffusion as determined by the MSE measurements.

The results are shown in figure 2. These show that the current diffusion calculated with neoclassical resistivity and experimentally measured Z_{eff} rapidly diverges from the measurements as seen in the q -profile in figure 2(d) and more directly by the MSE comparison in figure 2(b). This simulation shows a significant discrepancy for all radii greater than 3.1 m by as much as 2–3 times the magnitude of the experimental error. The simulation in which the electron temperature is increased by the maximum extent of its possible error range shows that the MSE data points and q -profile are moved towards the experimentally determined values, as expected, but that the shift is $< 10\%$ of the observed discrepancy and, in the case of the synthetic MSE data, the shift is significantly smaller than the quoted error on the experimental data. (It is noted that similar magnitude changes in MSE and q are found with only a change of the Z_{eff} value to $Z_{\text{eff}} = 1$. This data is not shown to prevent overcrowding the figure with similar data points.) An important point to note from this test is that the synthetic MSE data thus produced is still well outside the error range of the experimental MSE data when the maximum error has been applied to the T_e (or Z_{eff}). Therefore, although an exhaustive analysis of the error range of the synthetic MSE data has not been carried out, these tests demonstrate that measurement errors in the input data cannot account for the

observed discrepancy between modelling and experiment. It is found, however, that reasonable agreement between simulation and measurement is possible by using the combination of Spitzer resistivity with $Z_{\text{eff}} = 1.0$ in the simulation. This is shown particularly in figure 2(b) by the good match between the MSE measurements with the TRANSP simulated data with Spitzer resistivity (green squares) and the TRANSP simulation constrained to the EFIT q -profile (blue diamonds). The q -profiles do show some discrepancy at radii $R < 3.2$ m but the match of MSE points at all radii and of the q -profiles at $R > 3.2$ m is seen to be very good in this case. The mismatch in q -profiles for $R < 3.2$ m is attributed to the small plasma volume close to the magnetic axis (TRANSP $R_{\text{axis}} = 2.95$ m at $t = 41.9$ s) and correspondingly large uncertainty in current density in this region. The TRANSP calculations indicate less than 10% of the total plasma current is located in the core region with $R < 3.2$ m. There is also a small difference in Shafranov shift of the NCLASS simulation compared to the Spitzer simulation and the simulation with fixed q -profile. The maximum difference in Shafranov shift between the various TRANSP runs is 5 mm at the plasma magnetic axis, reducing as radius increases to a negligible level for $R > 3.2$ m. In a previous study of current diffusion in TFTR [25] it was found that TRANSP predicted a magnetic axis position that disagreed with the position of the peak in T_e profile by 4–5 cm. It was further suggested that a shift of this magnitude in the prediction of the current profile evolution would cause the prediction to match the experimental data. In the experiment presented here this assertion cannot be made since, early in the I_p ramp, the temperature profile can be very flat or even hollow so the position of the magnetic axis cannot be easily determined by observation of the T_e profile. Looking at the position of the magnetic axis calculated by MSE constrained EFIT and comparing this with the position calculated by TRANSP shows a mismatch of ~ 3 cm. However, the magnetic axis position calculated by TRANSP is similar for all three TRANSP simulations and the mismatch in position between TRANSP and EFIT is constant throughout the time evolution of the simulations. Therefore, it is not thought that errors in calculating the position of the magnetic axis are the source of the discrepancy in this case.

The calculated resistivity profiles are also shown in figures 2(e) and (f). In figure 2(e), the profiles all match well, confirming again that the initial condition of all the simulations is identical. In figure 2(f), the final states of the resistivity profiles are shown which largely confirms the observations drawn from the MSE data and q -profiles. The inferred resistivity from the simulation constrained to the EFIT q -profile is lower in the outer region of the plasma ($R > 3.4$ m). Interestingly, the inferred resistivity for $R < 3.4$ m is substantially higher than that calculated by NCLASS. However, since TRANSP indicates that $\sim 70\%$ of the total plasma current lies in the region with $R > 3.4$ m, it is thought that the principal source of the observed modelling discrepancy is the outer region of the plasma (i.e. $R > 3.4$ m) where the inferred resistivity is lower than that calculated by NCLASS. In agreement with the observations above, modification of just T_e in the simulations (or Z_{eff} , not shown) moves the calculated resistivity towards

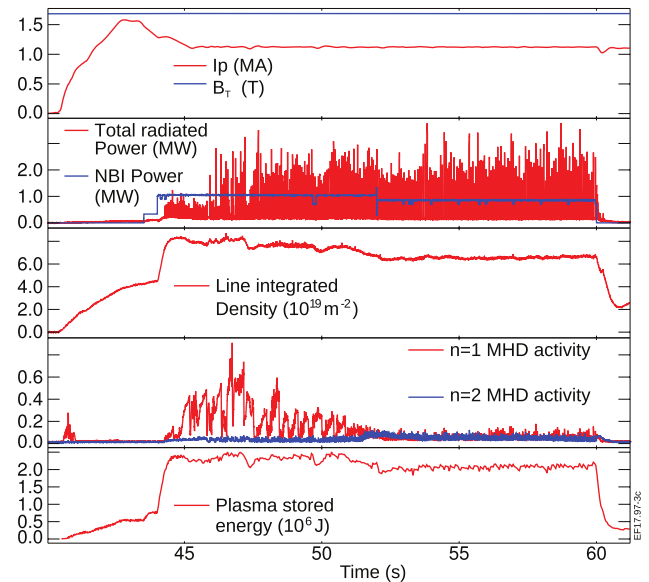


Figure 3. Time traces of principal plasma parameters for JET pulse 77280. Simulations are carried out during the 16 s NBI phase 44–60 s. MHD activity, line-integrated density, and plasma stored energy indicate the plasma reaches a stationary-state from ~ 53 s to the end of the NBI heating phase.

the inferred resistivity but only by a small amount. Changing to Spitzer classical resistivity with $Z_{\text{eff}} = 1$ matches the calculated resistivity with the inferred values for $R > 3.4$ m. It is further noted that it is not thought that changing the value of Z_{eff} combined with using Spitzer classical resistivity genuinely reflects the physics of the plasma being modelled in this case (for instance, the carbon content of the plasma is certainly non-zero and the resultant Z_{eff} is substantially larger than 1.0, even allowing for measurement error) but rather is a convenient way to illustrate the magnitude of the observed discrepancy between modelling and experiment.

2.2.2. JET stationary-state experiment. As a comparison to the early I_p ramp experiment, a stationary-state plasma was selected for similar analysis to determine whether such a discrepancy is seen when the plasma current profile is in a fully relaxed state. Time traces of principal quantities of the selected plasma discharge are shown in figure 3. This pulse was designed as part of a series investigating the hybrid mode and was intended to run for as long as possible in H-mode to allow the current profile to fully relax. As can be seen in the second panel of figure 3, the 10 MW of NBI heating applied was split into two sections, each section supplied by a separate beamline allowing the H-mode phase duration to be twice as long as the pulse-length limit of each individual beamline. Since only one NBI injector line-of-sight is viewed by the MSE diagnostic, MSE measurements are only obtained during the half of the heated phase during which the appropriate injector is switched on. For this reason, the pulse was repeated with the order of the beamlines swapped and the MSE measurements from the two pulses were considered to be representative of both plasmas. Examination of principal measurements from the two pulses indicates that they were essentially identical.

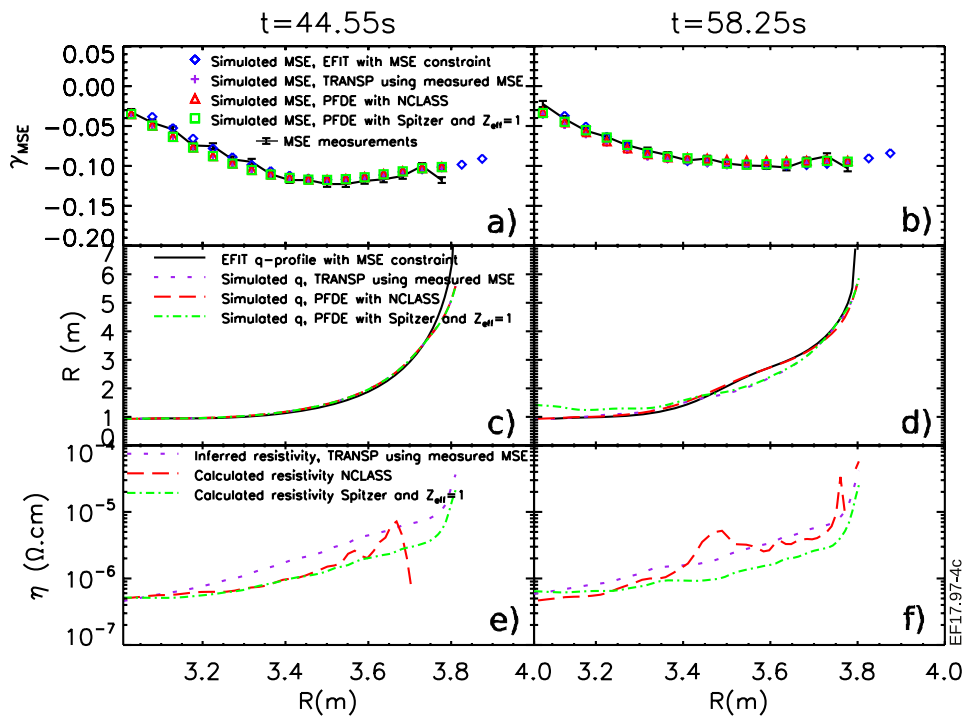


Figure 4. Measured and synthetic MSE profiles at the start (a) and end (b) of the simulation period (44.5–58.5 s) and corresponding q -profiles (c) and (d) and resistivity profiles (e) and (f). Full description of traces as in caption to figure 2.

The MHD activity in these pulses indicates that initially large sawteeth gradually reduce in amplitude and cease at around 51.5 s as the current profile relaxes. The pre-NBI current relaxation timescale in these plasmas was estimated to be ~ 0.9 s [49]. The presence of sawteeth was therefore not accounted for in the current diffusion modelling since it can be expected that there would be no residual effect on the current profile after several current diffusion times due to their presence earlier in the pulse. The results of the modelling are shown in figure 4. At the start of the simulation, as in the current ramp experiment, the q -profiles as shown in figure 4(c) are seen to be in good agreement with that obtained from MSE-constrained EFIT. Likewise, the associated synthetic MSE data, shown in figure 4(a), from EFIT and the TRANSP simulations are also in good agreement with the experimental measurements. The resistivity profiles at the start of the simulation, as shown in figure 4(e), are in reasonable agreement. The TRANSP simulations were run as before, allowing the current profile to evolve according to the poloidal field diffusion equation (PFDE) from the start time, 44.55 s, just after the main heating was switched on. The profiles were then re-examined at a much later time just before the main heating is switched off at 58.25 s when the current profile can be considered to be fully relaxed and any residual effect on the current distribution from the effect of the sawteeth earlier in the pulse will have dissipated. The q -profiles at the later time are shown in figure 4(d) and associated MSE data in figure 4(b). The simulation with best agreement to the EFIT generated q -profile is the one using NCLASS neoclassical resistivity which shows $q_{\text{min}} \sim 1$. This is a reasonable value given the observation that no sawteeth were present at this time. The simulation with Spitzer resistivity and $Z_{\text{eff}} = 1$ produces a

disagreement in the core ($R < 3.4$ m) where the modelled value of q was higher than that from MSE-constrained EFIT. The resistivity profiles at the end of the simulation run show that both TRANSP simulations are in reasonable agreement for $R < 3.4$ m but that for $R > 3.4$ m, the NCLASS calculation is a better match to the resistivity inferred from the run constrained to the EFIT q -profile. Interestingly at larger radius ($3.5 \text{ m} < R < 3.7 \text{ m}$) the q -profile from the simulation using Spitzer resistivity coincides with the simulation in which the q -profile is set to match that produced by MSE-constrained EFIT. In both of these cases, the Shafranov shift was slightly different to that seen in the NCLASS case by ~ 7 mm in the centre with the difference reducing towards larger radii out to $R = 3.5$ m. This is assumed to be the reason for the synthetic MSE data agreeing with measurements in all 4 cases whilst the q -profiles and resistivity profiles differ slightly. As mentioned in the previous section, it is not thought that this small discrepancy in the Shafranov shift is responsible for the discrepancy in q -profile and MSE profile in the I_p ramp-case.

2.3. MAST experiments

For the experiments on MAST, a different approach had to be taken as regards firing the neutral beam to obtain MSE measurements. With a comparatively small plasma volume, any NB injection on MAST produces a significant fast-ion density with respect to the thermal plasma so the neutral beam could not be considered non-perturbative to the plasma for any significant period of time. Therefore, any measurements taken after the first few milliseconds of beam-on time cannot be considered representative of the ohmically heated plasma.

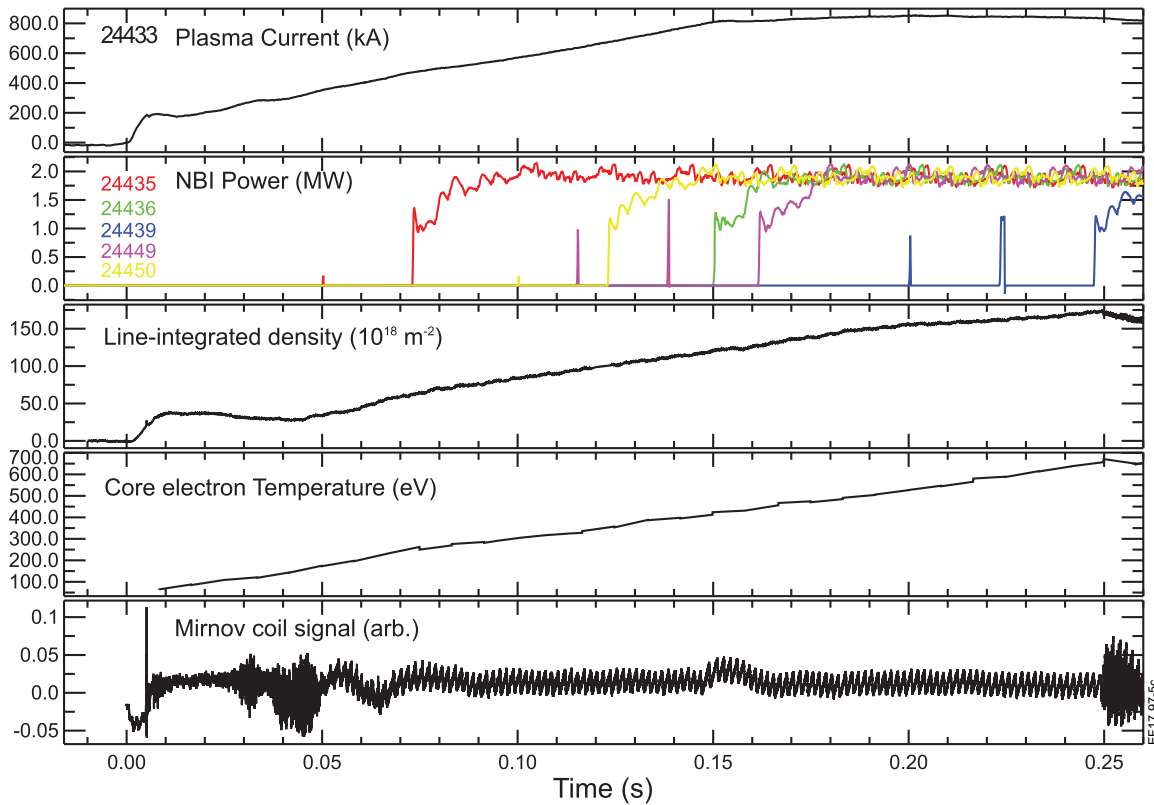


Figure 5. Time traces of principal plasma parameters for MAST pulse 24433 and NBI traces from subsequent pulses used to supply MSE ‘snapshots’ of identical plasmas at various times. Simulation is started at 0.075 s, half way through the I_p ramp-up phase. The bottom panel indicates that the period chosen for the simulation 75–252 ms does not exhibit any significant MHD.

In the initial set of experiments, it was decided that the good repeatability of MAST plasmas would be exploited to perform a series of plasma pulses which were identical except for the start time of the NBI heating. In each shot, the MSE measurements taken in the first 2 ms after the beam was switched on were considered representative of the ohmically heated plasma up to that point. This assumption is valid as the MSE diagnostic takes measurements on a much faster timescale than the slowing down time of the NB fast-ions in the plasma, typically 10–15 ms during the I_p ramp-up phase, hence the measurement is taken before the FI population is established and before the beam has heated the plasma significantly. A sequence of plasma pulses was thus executed with different NBI start times providing a series of ‘snapshots’ of the MSE profile of otherwise identical plasmas. The profiles recorded could then be compared with modelling of a final repeat of the same plasma in which no NBI was applied.

2.3.1. MAST I_p ramp-up. The plasma scenario chosen for the I_p ramp-up investigation was one of the eight standard scenarios developed for MAST experiments and therefore represented a commonly used plasma scenario. This consisted of an I_p ramp to 800 kA flat-top at full field ($B_T = 0.58$ T) and moderate density as shown in figure 5. The neutral beam waveforms from the shots making up the scan are shown in the second panel of figure 5, the start time of each indicating each MSE ‘snapshot’; a total of 6 useful MSE ‘snapshots’ were taken concentrating on the latter half of the I_p ramp-up and the I_p

flat-top. The TRANSP code was once again used to model the current diffusion, using the q -profile from MSE-constrained EFIT as an initial condition for the PFDE calculation. In these simulations, the Sauter neoclassical formulation [45, 46] was used as this had previously been shown to give marginally better agreement than NCLASS when assessing stationary-state ohmic plasmas on MAST [47]. The analysis period was defined by observing the MHD signals from the shots in the scan and selecting a start time after which no significant MHD is measured. The end time of the analysis period is similarly defined as being just before an MHD event is observed, after which that the current distribution in the plasma can no longer be considered to be governed by the simple diffusive process modelled. The bottom panel in figure 5 displays the signal from one of the Mirnov coils illustrating the absence of significant MHD during the analysis period: 75 ms–252 ms. The required input data for the TRANSP simulation were taken from standard MAST data from the shot with no neutral beam heating during the analysis period (MAST pulse 24433). The principal data (I_p , temperature and density profiles etc) from all other shots were compared to this and were found to be virtually indistinguishable up to the time in each shot when the NBI was switched on. The data from the NBI-free shot was pre-processed to ensure self-consistency in mapping to a common radial co-ordinate and the TRANSP simulation running the q -profile forwards in time by solving the PFDE. The simulated q -profile may then be compared with MSE-constrained EFIT

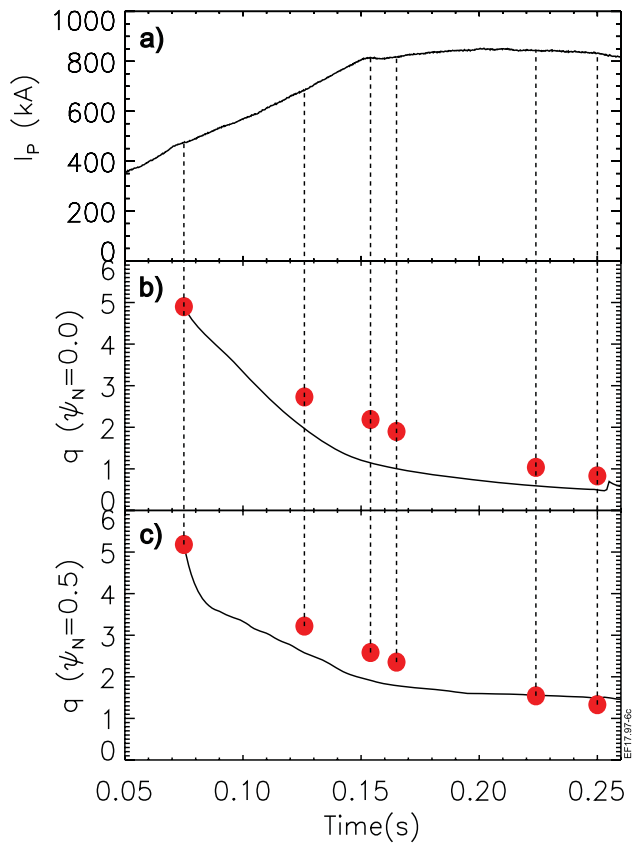


Figure 6. Simulation results for MAST pulse 24433 using TRANSP PFDE and Sauter neoclassical resistivity. (a) Plasma I_p ; (b) q at magnetic axis from TRANSP/PFDE simulation (black line) and MSE-constrained EFIT (red spots); (c) q at half radius from TRANSP/PFDE simulation (black line) and MSE-constrained EFIT (red spots).

at the times of later MSE snapshots and the simulated MSE profile may be directly compared with the measurements at these later times.

The results comparing simulation and experiment are shown in figures 6 and 7. Examination of the results in figure 6 shows that the simulated q -profile rapidly diverges from that produced by MSE-constrained EFIT, with much lower values of q in the core of the plasma than shown in the EFIT analysis. This situation, with lower q in the plasma core persists until the end of the analysis period. The lower q in the simulations corresponds to a more rapid inward diffusion of current density in the simulation than implied from the EFIT analysis. Comparisons of the profiles of measured and simulated MSE data are shown in figure 7 along with the q -profiles and resistivity profiles at these times. Four sets of data are included in each axis corresponding to the experimental MSE data, a TRANSP run in which the q -profile was constrained to match the EFIT q -profile, and the TRANSP run evolved using the PFDE. In addition, a run with T_e increased to the maximum extent of its error range is shown. On the left-hand side, it is seen that the TRANSP simulation runs match the MSE data well at the initiation of the run at 75 ms (figure 7(a)) and the q -profiles from the TRANSP simulations also match the EFIT q -profile well (figure 7(c)). The resistivity profiles for the initial condition also match well (figure 7(e)). By the

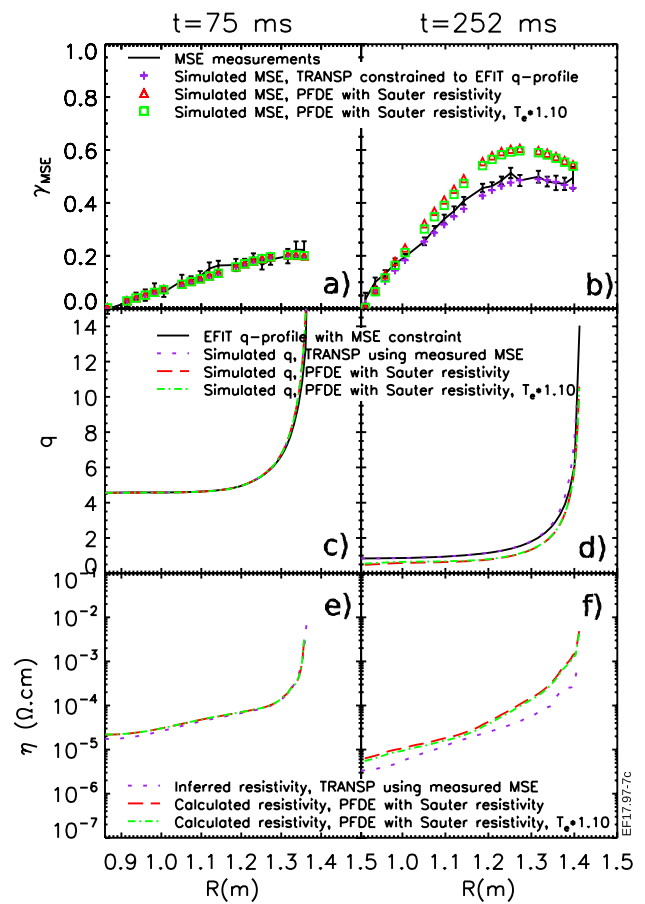


Figure 7. Radial profiles of measured and synthetic MSE data at the start and end of the TRANSP simulation for MAST pulse 24433. (a) MSE measurements with error bars at the start of the simulation period, 75 ms, with simulated MSE data from: TRANSP with q -profile required to match EFIT MSE constrained q -profile (purple crosses); TRANSP with q -profile evolved by poloidal field diffusion equation (PFDE) using Sauter neoclassical resistivity (red triangles); TRANSP with q -profile evolved by PFDE using Sauter neoclassical resistivity and $T_e \times 1.10$ (green squares). (b) MSE data, as described for panel a), at the end of the simulation run time: 252 ms. (c) q -profiles from MSE-constrained EFIT and the TRANSP simulations described above at the start of the simulation period. (d) q -profiles from MSE-constrained EFIT and the TRANSP simulations at the end of the simulation period. (e) Resistivity profiles from the TRANSP runs at the start of the simulation period. (f) Resistivity profiles from the TRANSP runs at the end of the simulation period.

end of the run at 252 ms, the simulated MSE of the PFDE run has diverged from the measurements such that it is well outside the range of the MSE measurement errors. Similarly, the q -profile does not match the EFIT q -profile, whilst the TRANSP run constrained by the EFIT q -profile does still match (and, indeed, the simulated MSE from this run matches the measurements) indicating that the mismatch in the PFDE run is unlikely to be attributable to any faults with the equilibrium solution produced by TRANSP. The same mismatch is seen in the resistivity profiles in figure 7(f) where resistivity calculated with the Sauter neoclassical model does not match that inferred from the run constrained to the EFIT q -profile. The run with increased T_e shows very little departure from the unadjusted simulation in figures 7(b), (d) and

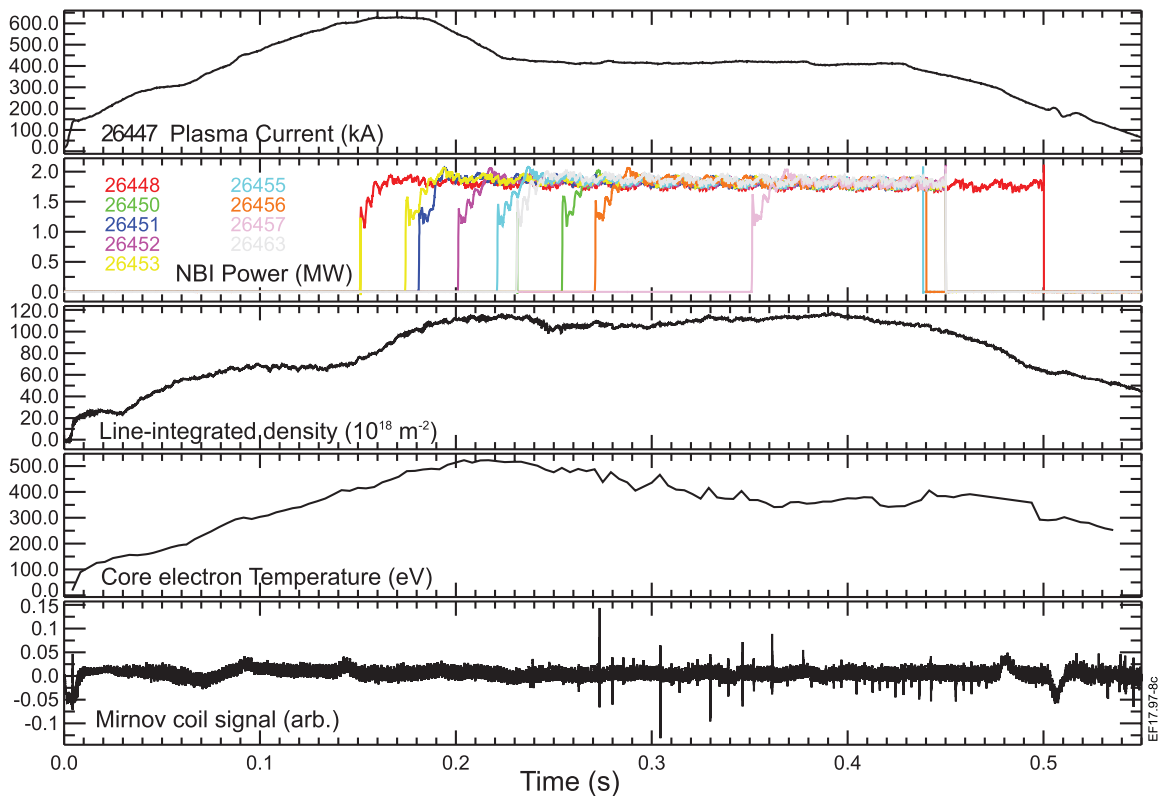


Figure 8. Time traces of principal plasma parameters for MAST pulse 26447 and NBI traces from subsequent pulses used to supply MSE ‘snapshots’ of identical plasmas at various times. Simulation is started at 0.150 s, at the start of the initial I_p flat-top phase. The bottom panel indicates that the period chosen for the simulation 150–274 ms does not exhibit any significant MHD.

(f) indicating that the mismatch is not simply due to errors in experimental measurement. It is again noted that the magnitude of the difference seen by setting $Z_{\text{eff}} = 1$ is similar to that seen when using T_e increased by 10% but that this has not been shown so as not to overcrowd the figure with similar data points. Furthermore, such an adjustment to Z_{eff} is a large overestimate of the error since a full 2D measurement of visible bremsstrahlung is available on MAST allowing a profile of Z_{eff} to be determined. This result is therefore similar to that seen in the JET ramp-up experiment detailed in section 2.2.1.

2.3.2. I_p ramp-down. The second MAST experiment was designed to test whether a similar discrepancy is seen when plasma current is ramped down from an initial flat-top. In this experiment, I_p was first ramped up to 600 kA, maintained at this level for 30 ms before ramping down to 400 kA and remaining at this level for several hundred milliseconds as illustrated in figure 8. The lower values of I_p used in this experiment were a compromise between the requirement to ramp to high enough current for an effective experiment and the available total flux swing of the central solenoid to produce a pulse of sufficient duration to perform the experiment. Eight repeats of this plasma were carried out resulting in eight MSE snapshots, starting during the first I_p flat-top and examining the I_p ramp-down and the second I_p flat-top as shown in the second panel of figure 8. The start-time of the analysis period in this experiment was defined by the start of the first I_p flat-top. The end time for the analysis was again defined by first significant MHD event which would perturb the current

distribution, however, the discussion below concentrates on the period where I_p is ramping down and the initial part of the second flat-top phase immediately after the ramp-down.

The same analysis procedure was applied, using a q -profile from MSE-constrained EFIT as the initial condition for the TRANSP simulations starting at 155 ms. Results are shown in figures 9 and 10. Once again it can be seen in figure 9 that the q -profile in the PFDE simulation rapidly diverges from that produced by the MSE-constrained EFIT i.e. the simulation overestimates the rate at which current diffuses suggesting that the effective resistivity is lower than the expected value. Interestingly, the value of q at the half-radius in the PFDE simulation (figure 9(c)) follows the EFIT- q rather well during the ramp-down compared with the ramp-up experiment in which the q -value in the centre and at the half radius fell faster in the PFDE simulation. In contrast, the value of q at the centre falls more rapidly in the plasma centre in the PFDE simulation. In this simulation, q_0 drops below 1 at about 200 ms, reaching 0.7 at around 225 ms which is certainly low enough to expect to observe sawteeth. Since no sawteeth were observed, it is expected that q_{min} did not drop below 1 for the entirety of the analysis period shown. The simulated MSE data shown in figure 10 (a) and (b) again shows that from the initial condition where the simulation is in good agreement with the measurements, the simulation rapidly diverges to a point where the simulated MSE data is well outside of the error range of the experimental data. As before, the synthetic MSE data from the simulation with constrained q -profile is still in good agreement with the measurements whilst the discrepancy in Shafranov

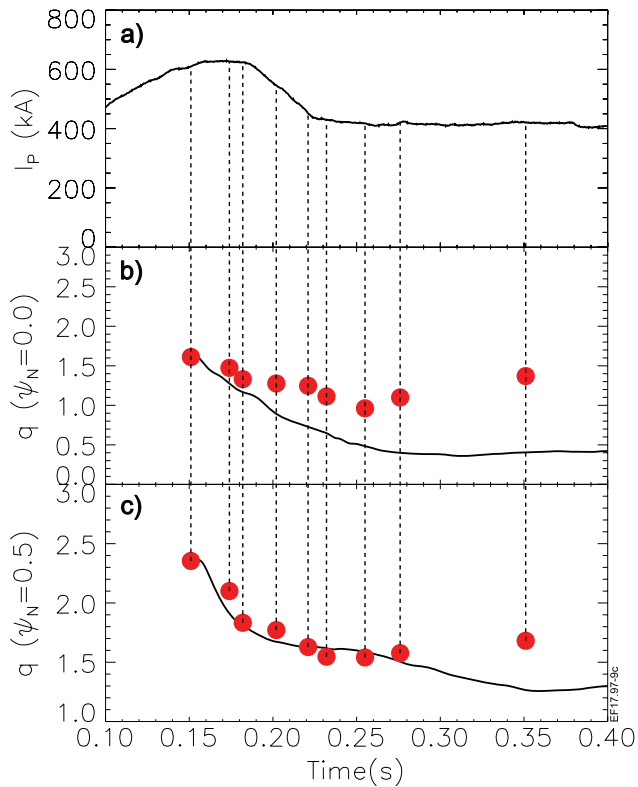


Figure 9. Simulations results for MAST pulse 26447 using TRANSP PFDE and Sauter neoclassical resistivity. (a) Plasma I_p ; (b) q at magnetic axis from TRANSP/PFDE simulation (black line) and MSE-constrained EFIT (red spots); (c) q at half radius from TRANSP/PFDE simulation (black line) and MSE-constrained EFIT (red spots).

shift between these simulations is <10 mm at the magnetic axis by the end of the simulation period, indicating that the disagreement in the PFDE simulation is unlikely to be due to a fault with the equilibrium solutions found by TRANSP.

The match between TRANSP and EFIT in $q_{0.5}$ for the first ~ 100 ms of the simulation, shown in figure 9(c), appears on examination of the current profiles to be a fortuitous choice of radius rather than because the current diffusion is being modelled correctly. In the MSE-constrained EFIT, the current density at the centre continues to rise until around 250 ms when the effects of the current ramp-down cause the current density on axis to fall and diffuse outwards, raising the current density off-axis to a value higher than would be expected for a simple monotonic I_p ramp followed by a flat-top. In the TRANSP PFDE simulation the current density diffuses inwards from all radii throughout this period leading to a highly-peaked profile at 315 ms. It appears that, at the half-radius, the current density seen in EFIT due to the inward-outward diffusion approximately matches the current density due to the monotonic inward diffusion in the TRANSP PFDE simulation, giving the agreement in the value of q at this radius seen in figure 9(c) until around 250 ms. It is clear though that, after this time, the TRANSP PFDE simulation is not a good representation of the current density at this radius, a conclusion corroborated by the mismatch between synthetic and measured MSE data shown at the later time in figure 10(b). It is therefore concluded that the TRANSP PFDE simulation with neoclassical resistivity

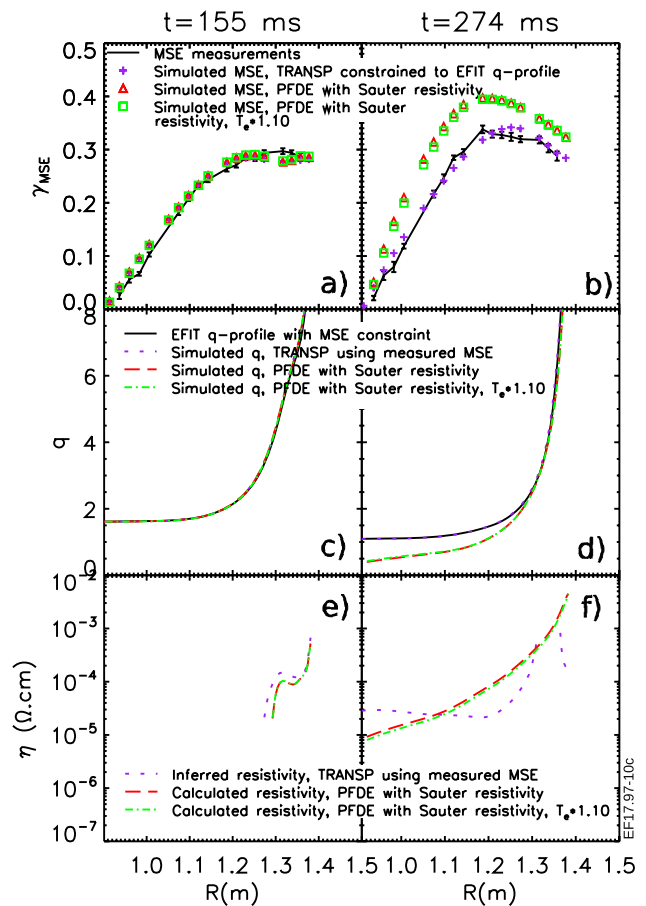


Figure 10. Radial profiles of measured and synthetic MSE profiles of MAST pulse 26447 at the start (a) and end (b) of the simulation period (150–274 ms) and corresponding q -profiles (c) and (d) and resistivity profiles (e)–(f). Full description of traces as in caption to figure 7.

does not accurately follow the evolution of the toroidal current profile observed in the experiment during the I_p ramp-down, in agreement with the current ramp-up result in the previous section.

2.3.3. MAST stationary state. The results presented in the previous sections suggest an issue with modelling current diffusion during dynamic phases where the plasma current is ramped up or down. The JET stationary-state experiment further suggested that modelling of the fully relaxed current profile produces a result well matched to experimental measurements. An experiment to test modelling of a fully-relaxed current profile on MAST was therefore motivated, in particular to provide confidence that modelling of expected current profiles in future devices such as MAST-U [50] is valid.

Reaching a stationary-state plasma is not possible in high I_p MAST plasmas as the limitations of the hardware mean that the pulse cannot run for sufficient duration for the current profile to reach a fully relaxed state. It was therefore decided that a lower current, $I_p = 400$ kA, ohmically heated plasma would be used as this would offer a sufficiently long I_p flat-top to reach a stationary-state which could be maintained for sufficient time for the current profile to fully relax. It is necessary to maintain stationary-state for several current-diffusion

times to ensure that a simulation in which the current profile diverges from measurements during the dynamic phase can continue to evolve the current profile for sufficient time that it may converge with the experimentally determined current profile at later times. The experiment was run twice, once at low density and again at high density allowing a comparison to be made between similar plasmas with varying collisionality and temperature. Due to constraints on available machine time, a newly commissioned function of the MAST NBI system [51] was utilised which allowed four short beam ‘blips’ to be fired with start-times and duration that could be specified to within ± 1 ms. Obviously it is desirable that such blips, intended for diagnostic measurements only, be kept as short as possible so as to perturb the plasma as little as possible. The MSE system operated at 100 Hz and required 5 ms integration time to produce a useable signal. Since the absolute timing of the MSE system could not be arbitrarily specified (i.e. it could not be synchronised with the beam blips) it was decided that the beam blips needed to be 11 ms duration to guarantee an MSE measurement within the beam-on time window. The beam slowing-down time in the target plasma scenario was calculated to be of the order of 15 ms so the beam blips were still shorter than the time required to build up a full F.I. distribution. Whilst it is recognised that a beam-on time of duration close to that of the beam slowing-down time is likely to result in a small but noticeable level of heating, it was felt that this represented a reasonable compromise in order to be able to execute the experiment and take meaningful data. In the low-density plasmas, EFIT shows plasma stored energy of ~ 13 kJ, rising to ~ 20 kJ with each beam blip and decaying back to the pre-injection level on a beam slowing down timescale. In the high-density plasmas, EFIT shows plasma stored energy of ~ 16 kJ rising to ~ 22 kJ with each beam blip and decaying on a beam slowing down timescale. Each of the high and low density plasmas was repeated once with the beam-blips at different times so that, again utilising the repeatability of MAST plasmas, a total of 8 MSE measurements-per-scenario were obtained, with the first measurement soon after the start of the I_p flat-top and the rest regularly spaced for the several hundred milliseconds of the flat-top duration. The experiments and timing of the beam blips and associated MSE measurements are illustrated in figure 11.

The analysis of this experiment was conducted similarly to that already described in the preceding sections using the TRANSP code. A slight difference in this case was that the NUBEAM module was employed within the TRANSP simulation to account for the small amount of heating and possible low-level of neutral-beam current-drive that may result. This was necessary in this case as the TRANSP analysis continued after each NBI blip so it was important to account for this small effect on the plasma. In the previous experiments, by contrast, a purely ohmic plasma was run for the full time-dependent analysis and the NBI heated shots were only used to supply the single time-point MSE data. The results of the analysis are shown in figures 12–14.

Firstly, it is clear that a successful simulation must incorporate some model for the regular $n = 1$ sawteeth that occur from 250 ms onwards in the low-density scenario and from

200 ms onwards in the high-density scenario. Without such a model in place to redistribute the core current, a central value of q well below 1 would result with a $q = 1$ radius much larger than would be expected in the real plasma. For the simulations presented, the Kadomtsev reconnection model was employed with a sawtooth frequency of 100 Hz in the low-density experiment and 150 Hz in the high-density experiment, determined by observation of the MHD signal from the experiment. Figure 12(b) shows that, from the simulation start time at 155 ms, the simulated value of q_0 drops to $q = 1$ faster than in the real plasma reaching $q = 1$ at $t = 165$ ms in the low-density case and at $t = 185$ ms in the high-density case. In the experiments, by contrast, the appearance of the first sawtooth in each case, at the later times stated previously, is indicated by an inversion in the soft x-ray signals and by a discontinuity in the line-integrated density signal. This observation, of faster modelled inward current diffusion than observed in the experiment, is generally in agreement with the results shown in the previous sections as, in this phase of the plasma evolution, the current profile is still in the process of evolving towards a relaxed state. Analysis of the soft x-ray signals indicate that the inversion radius of the sawteeth occurs at approximately $\rho \sim 0.35$ (where ρ is normalized poloidal flux).

Examination of the evolution of q at the axis and the half-radius in figures 12(b) and (c) shows that approximately 100 ms after the appearance of the first sawtooth, the plasma has evolved close enough to a stationary state that the simulated q -profile is largely in agreement with that derived from MSE-constrained EFIT. This is further confirmed by the match, to within experimental errors, of the simulated and measured MSE and q -profiles shown in figures 13(b), (d) and 14(b), (d). Since the current distribution in the core of these plasmas inside the radius $\rho < 0.35$ is strongly affected by sawteeth, any match between simulation and experiment in this region only confirms that the MHD model used for current redistribution is appropriate. Outside this region however, the current profile should still be expected to result from current diffusion with an appropriate resistivity model. The match of the MSE data with the simulation at the advanced times when the current profile outside $\rho > 0.35$ should be fully relaxed confirms that the neoclassical resistivity model is a good description of the plasma outside the region affected by the sawteeth in the stationary state. It is noted that a small discrepancy exists in the high-density data for radii $R > 1.25$ m though the simulation result is still in much better agreement than the equivalent dynamic experiments shown in previous sections. These conclusions are also supported by the resistivity profiles shown in figures 13(f) and 14(f) which show a good match between the resistivity calculated using the Sauter neoclassical model and that inferred from constraining the simulation to the EFIT q -profile.

This result provides confidence that simulations of the current profile of stationary-state plasmas can be considered reliable but that the timescale to reach that stationary-state (at least in terms of the simulated current profile relaxation) could be significantly longer than the dynamic phase of a simulation would otherwise suggest.

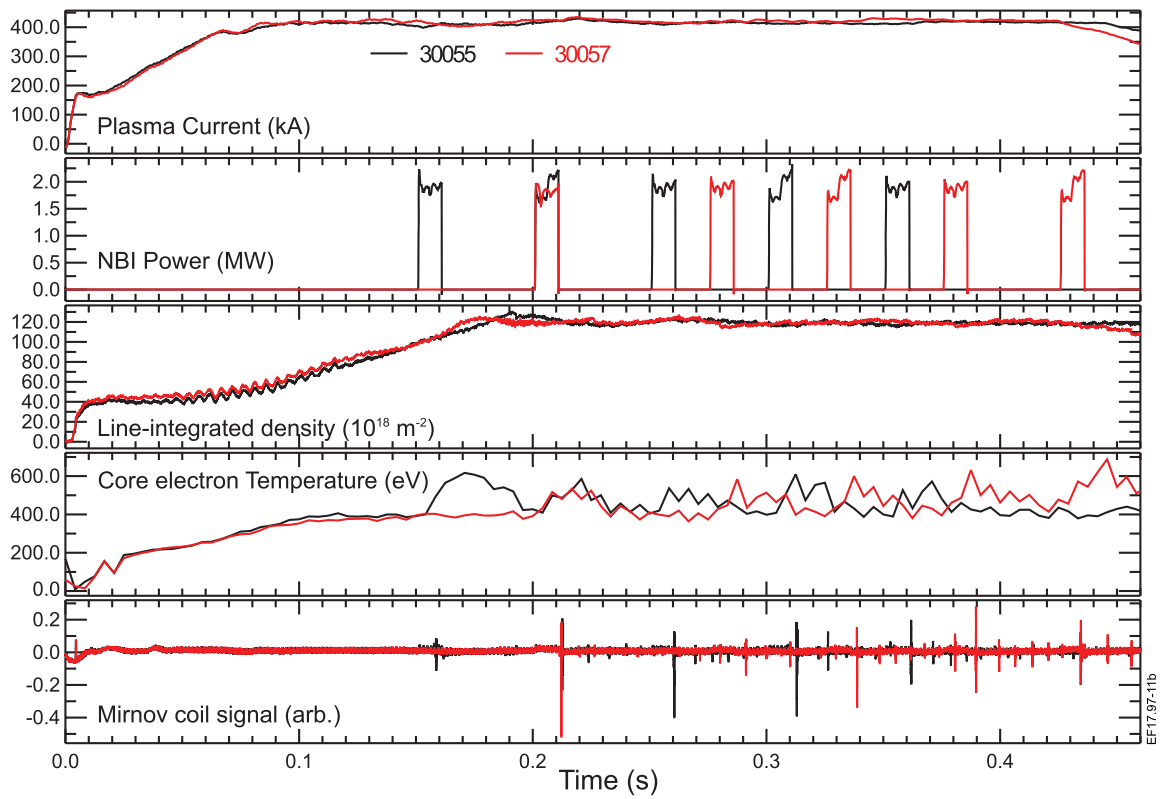
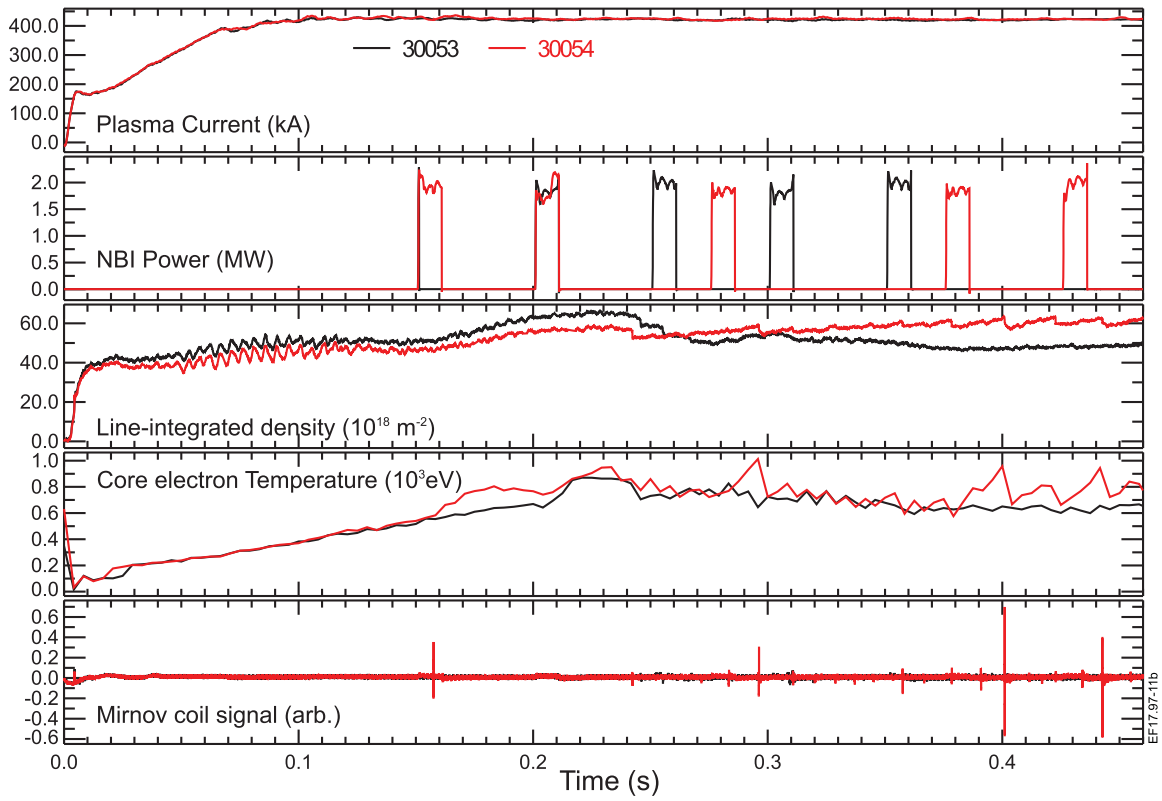


Figure 11. Principal traces from the low density (30053, 30054, top) and high density (30055, 30057, bottom) stationary state test shots on MAST.

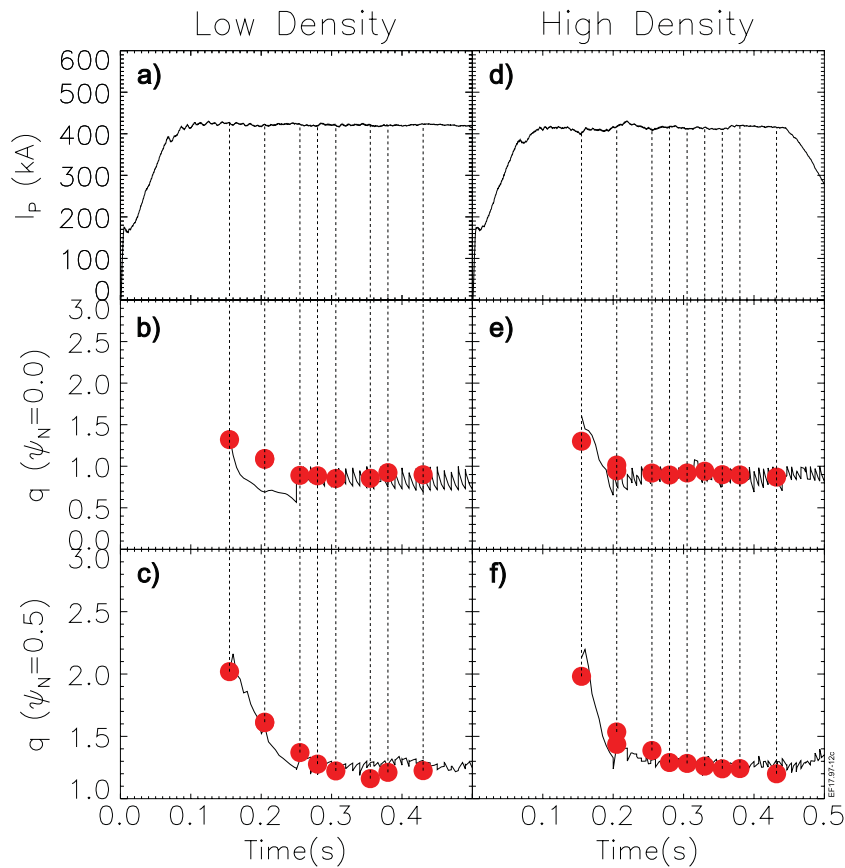


Figure 12. Simulations results for MAST pulses 30053 (low density) and 30055 (high density) using TRANSP PFDE and Sauter neoclassical resistivity. (a) Plasma I_p ; (b) q at magnetic axis from TRANSP/PFDE simulation (black line) and MSE-constrained EFIT (red spots); (c) q at half radius from TRANSP/PFDE simulation (black line) and MSE-constrained EFIT (red spots). (d)–(f) Same data for high density pulse.

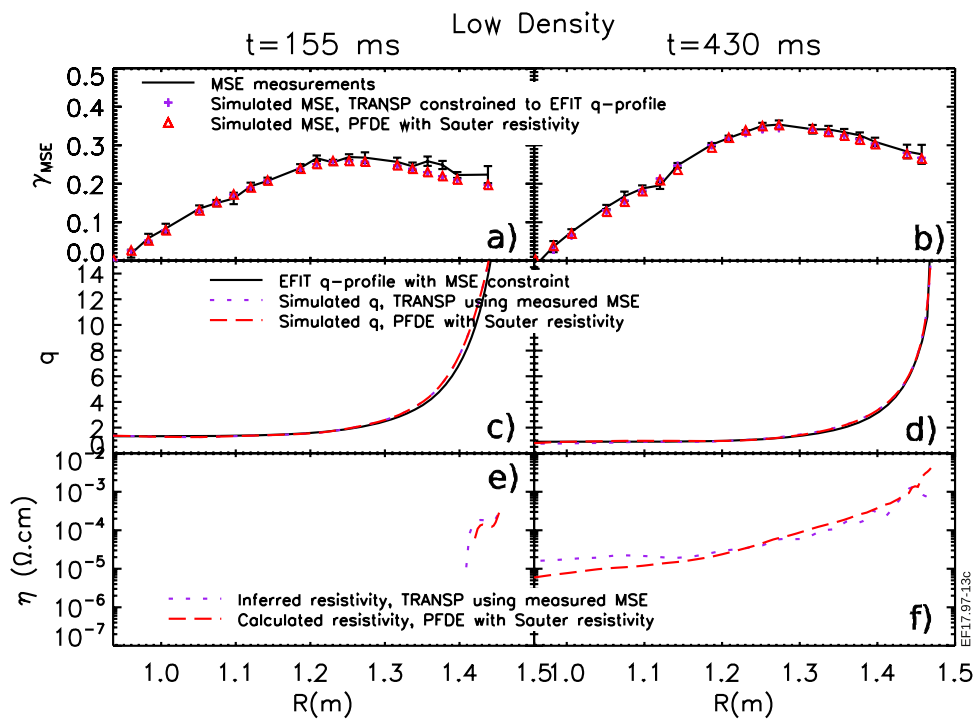


Figure 13. Radial profiles of measured and synthetic MSE profiles of MAST pulse 30053 at the start (a) and end (b) of the simulation period (155–430 ms) and corresponding q -profiles (c) and (d) and resistivity profiles (e) and (f). Full description of traces as in caption to figure 7.

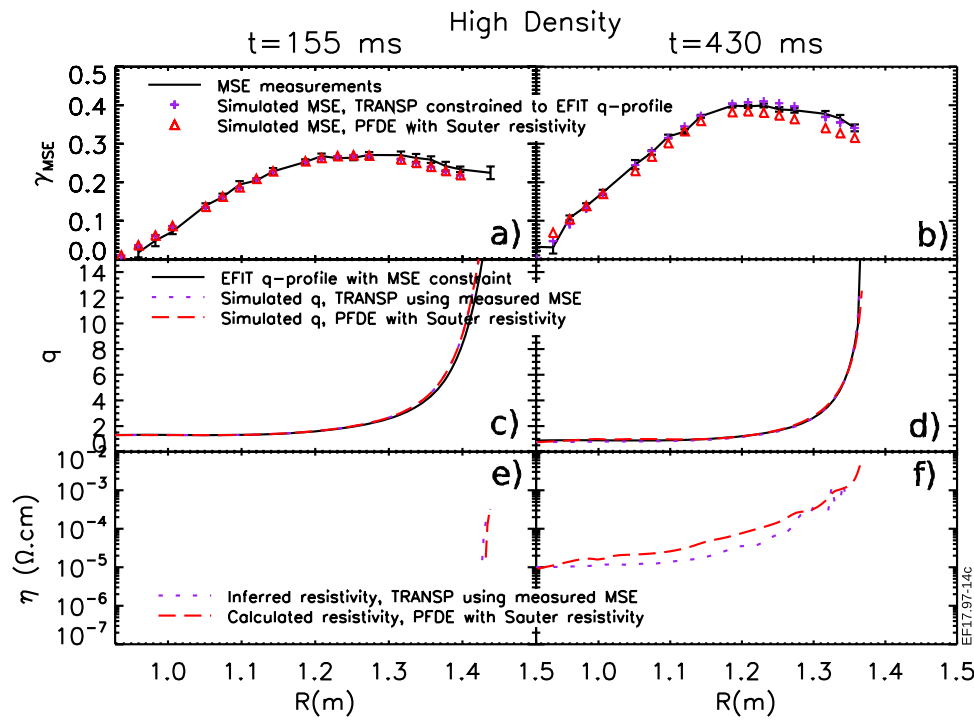


Figure 14. Radial profiles of measured and synthetic MSE profiles of MAST pulse 30055 at the start (a) and end (b) of the simulation period (155–430 ms) and corresponding q -profiles (c) and (d) and resistivity profiles (e) and (f). Full description of traces as in caption to figure 7.

3. Resistivity comparisons

In the previous sections simulation results from the TRANSP code have been presented detailing the current diffusion calculations carried out within the code using the neoclassical resistivity model, and in the JET experiments, additionally with the classical Spitzer formulation. In this section, the resistivity profiles themselves will be examined in more detail. When the TRANSP code is run in the mode in which a match to the supplied q -profile is required, a convenient output is the inferred resistivity. That is, assuming a reliable q -profile is supplied to the code such as that produced by MSE constrained EFIT, the inferred resistivity profile is then that which would be required for the PFDE to reproduce the experimentally observed current diffusion. This profile may then be compared to those calculated using the classical and neoclassical formulations. In order to validate the resistivity model in TRANSP, the resistivity profiles of the JET and MAST I_p ramp-up experiments were calculated using a different code. Performing this calculation independently of the TRANSP environment and obtaining a similar answer (as will be shown) provides an important check that there are no errors associated with the calculation.

Having recently installed the NEO code [48] at Culham, this was selected to carry out the comparison of the resistivity calculation. A time-dependent version of NEO was not yet available at the time of this study so the comparison between NEO and TRANSP focussed on the calculation of the resistivity profile at a particular time. It is to be emphasised that the purpose of this comparison is not to test the physics formulated by NEO but rather to verify the neoclassical resistivity calculations produced by TRANSP and NCLASS/Sauter.

Finally, a technique for calculating inferred resistivity directly from EFIT equilibria was employed to validate the TRANSP inferred resistivity calculation. This technique, developed by Forest *et al* [24] will be referred to in the following discussion as the Forest method.

The JET pulse 79649 was again used for this test at time $t = 41.6$, i.e. the start time of the TRANSP simulations, with standard input data for density, temperature, Z_{eff} and equilibrium information taken from EFIT. Two calculations of the resistivity profile were then made with NEO, the first with the experimental value for Z_{eff} , the second with $Z_{\text{eff}} = 1$ to test the sensitivity of the calculation to this quantity. The Forest method was also employed to produce an estimate of the resistivity profile directly from EFIT for comparison with the TRANSP inferred resistivity calculation. Similarly, the MAST ramp-up pulse, 24432, was used to make the comparison between TRANSP and NEO for the MAST device. Again, two NEO calculations were carried out with experimentally obtained Z_{eff} and with $Z_{\text{eff}} = 1.0$, and the Forest method was used to obtain the inferred resistivity from EFIT. This methodology calculates $\langle \mathbf{E} \cdot \mathbf{B} \rangle$ and $\langle \mathbf{j} \cdot \mathbf{B} \rangle$ from the time derivative of the poloidal flux produced by EFIT from which, assuming negligible noninductive current drive, the resistivity can be obtained. This is a reasonable approximation since, in the MAST I_p ramp-up experiments, the total noninductive current fraction (estimated from TRANSP) is $\sim 3\%$ of the total toroidal current whilst for the JET I_p ramp-up experiments it is 5% for the times shown in figure 15. The calculated resistivity profile is implicitly an average over each discrete time period between successive EFIT time-slices. The interval between successive time points must be selected such that the derivative is taken over a long enough period that it is not unduly

affected by signal noise in the input data used to produce the EFIT equilibria and not so long a time that the details of the evolution of the current profile are lost in the time average. For the JET experiment, the time-period of interest is 500 ms and the characteristic current diffusion time is ~ 0.9 s. Therefore, periods of ~ 50 ms between successive timeslices were selected as fulfilling the above criteria. This is significantly longer than the sampling period of the diagnostics used as input data to EFIT but short compared to the characteristic current diffusion time. For the MAST I_p ramp-up experiments, the EFIT timescale was necessarily constrained by the number of MSE ‘snapshots’ available as described in section 2.3. This sparser dataset still produces a reasonable representation of the resistivity profile since the characteristic timescale for current diffusion in these plasmas is estimated at ~ 0.6 s [49]. The shorter calculation periods of, typically, 25 ms from the EFIT analysis are still appreciably longer than the diagnostic sampling time and shorter than the characteristic current diffusion time; the calculation therefore captures the dynamics of the current diffusion and yields a useful result. The resistivity profiles thus calculated are shown in figure 15 along with those taken from the equivalent TRANSP simulations. The traces taken from TRANSP include the calculation according to the NCLASS neoclassical model, the calculation according to the Spitzer (classical) model and the resistivity inferred from the imposition of the particular q -profile as described above.

First, examining figure 15(a), it can be seen that there is a good agreement between the resistivity calculated by NCLASS in TRANSP and that calculated by NEO. The resistivity from the classical Spitzer formulation is lower than the two neoclassical calculations over most of the profile, as expected. The resistivity inferred from the TRANSP run including the experimental q -profile constraint is seen to be significantly lower than the neoclassical and the Spitzer calculations in the region $\rho_T > 0.45$ and appreciably larger at radii $\rho_T < 0.4$ (where ρ_T is the square root of normalized toroidal flux). The core of the plasma at small radius represents a small proportion of the total toroidal plasma current so resistivity calculated or inferred in this region should be expected to be subject to large error. Less than 10% of the total toroidal current is contained within the region $\rho_T < 0.3$ and, by comparison, approximately 70% of the total current is contained in the region $0.3 < \rho_T < 0.8$. Therefore, the comparisons at larger radii are of much greater significance to this discussion than the core region. A full quantitative analysis of the error magnitude would require a Monte-Carlo type approach with the input data to EFIT, which is beyond the scope of this investigation. An estimate of the maximum error can be inferred from the resistivity profiles calculated from neoclassical with experimental Z_{eff} and neoclassical with $Z_{\text{eff}} = 1$, which shows that even this large change to the input data to the TRANSP calculation does not bring the resistivity profile into line with the inferred resistivity profile at large radius. At larger radii, particularly in the region $0.6 < \rho_T < 0.8$, the departure of the inferred resistivity from either the neoclassical or Spitzer calculations indicates that the discrepancies so far observed have causes that go beyond the applicability of either the one model or the other. The

Forest method calculation shows a resistivity value lower even than the TRANSP inferred resistivity in the region $\rho_T > 0.40$, at smaller radii, the Forest method calculated resistivity goes negative, a result that is clearly unphysical. Since TRANSP calculates an internal equilibrium during execution, it is not surprising that the TRANSP inferred resistivity and the Forest method calculated resistivity, based on an equilibrium calculated by EFIT, do not match. The two calculations are consistent, however, in that they both show a resistivity lower than classical or neoclassical calculations for radii $\rho_T > 0.45$. In figure 15(c), a similar set of calculations is presented, this time setting $Z_{\text{eff}} = 1.0$ in the TRANSP calculations. The neoclassical calculation from NEO, the inferred resistivity calculation from TRANSP and the Forest method calculated profile are the same as in figure 15(a) for ease of comparison of the TRANSP results. In these simulations, it is observed that changing the Z_{eff} reduces the calculated resistivity so that it is now closer to the inferred value for both neoclassical and Spitzer for $\rho_T < 0.9$. The Spitzer value however is the best match, agreeing with the results shown in section 2.2.1. It is noted once again that the better match of the Spitzer-with- $Z_{\text{eff}} = 1.0$ simulation does not indicate that it is believed that no impurities are present in the plasma. Rather, it indicates the extent to which the current diffusion model must be modified, through the incorporation of additional physics, for agreement with experiment to be achieved.

Similar results from the MAST I_p ramp-up case are presented in figures 15(c) and (d). In figure 15(c), the calculation of neoclassical resistivity from TRANSP and NEO are again in good agreement. In this case the Spitzer resistivity profile is significantly different to the neoclassical calculations owing to the larger trapped particle fraction generally present in spherical tokamaks compared to conventional aspect ratio. As in the results for the JET I_p ramp-up, the inferred resistivity is lower than the Spitzer calculation and the Forest method calculation is consistent with the TRANSP inferred resistivity at large radii ($\rho_T > 0.6$) though has a value consistent with the neoclassical models at smaller radii, $\rho_T < 0.25$. However, as previously noted, calculation errors should be expected to be larger at smaller radii with $\sim 10\%$ of the total toroidal current contained in the region $\rho_T < 0.2$. Examination of figure 15(d), in which $Z_{\text{eff}} = 1$ was imposed in the TRANSP simulations indicates that even this modification is insufficient to match the inferred resistivity profile. It is observed that the resistivity goes negative for radii $\rho_T < 0.4$ which, again, is clearly unphysical.

The discrepancy between the inferred and calculated resistivity, and the fact that the inferred resistivity in some cases has a negative value strongly suggests that a purely diffusive model for the poloidal field evolution is not applicable. Possible explanations include an additional source of toroidal current, or the neglect of other terms in the generalized induction equation. Concerning the possibility of a toroidal current source, an obvious candidate would be a runaway electron current. However, no high-energy x-rays were detected during these experiments, which would be expected in the presence of runaway electrons, and calculations indicate that the condition specified by Dreicer [52] for the appearance of a runaway electron beam is not satisfied in these plasmas.

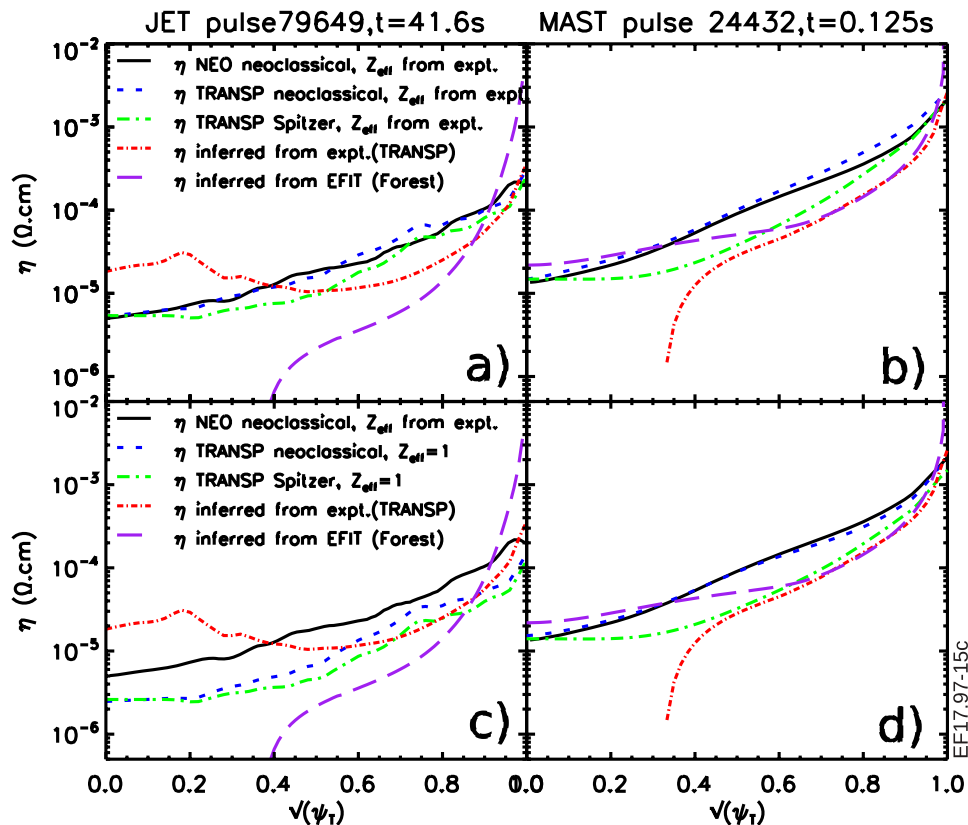


Figure 15. Resistivity profiles from NEO, TRANSP and from the Forest method calculation (see text for details) for JET pulse 79649 (a) and (b) and MAST pulse 24432 (c) and (d). For JET, the TRANSP neoclassical calculation is from NCLASS, for MAST TRANSP neoclassical is from Sauter.

4. Discussion

In the previous sections it has been shown in detail how a common technique used to model the dynamics of current diffusion in tokamak plasmas does not match the experimental observations of current diffusion during dynamic phases of the plasma current evolution. Care was taken when designing the experiments to ensure no significant or measurable MHD was present in the plasmas analysed which would otherwise invalidate the assumption of the current evolution being due to a purely diffusive process. It can therefore be stated that the disagreement shown is not thought to be simply due to MHD activity. Other processes that are not captured in the diffusive model used may be responsible e.g. strong flows or non-MHD effects such as a neglected Hall term, electron inertia, pressure gradient or turbulence effects. A next step in this investigation could be to attempt to include these effects in the current diffusion calculation similarly to the way the ‘hyper-resistive’ term was included in previous studies [30].

What is particularly interesting is the comparison between JET, a large conventional aspect ratio device and MAST, a considerably smaller tight-aspect ratio device. In the plasmas examined, there is some difference in collisionality but, in the tight-aspect ratio device, the particular difference is the neoclassical trapping fraction which, according to the TRANSP calculations performed, rises to $\sim 70\%$ at large radius in JET but in MAST is over $\sim 90\%$ at large radius. Even with this difference, and the effect it has in the neoclassical resistivity

calculation, the discrepancy observed in the current diffusion calculation is similar in the two machines with inward current diffusion proceeding more rapidly in the simulations than observed in experiment.

In contrast, simulations of stationary-state plasmas indicated that the current diffusion model using neoclassical resistivity did reproduce the observed current profiles, as confirmed by simulated and measured MSE. In the MAST plasmas, this was in the presence of sawteeth, the effects of which were modelled using Kadomtsev reconnection, meaning that the current diffusion was only valid at larger radii, $\rho > 0.35$. In JET, the plasma evolved to an MHD-free state and the plasma current profile was well reproduced by the model using neoclassical resistivity.

The implications of these findings for modelling current evolution in future devices are two-fold. In the first instance, the stationary-state modelling lends confidence that any stationary-state prediction can be considered reliable as the tests detailed in this article confirm. In the dynamic phase of the plasma evolution however, it is possible that predictive simulations of I_p ramp-up in particular may be calculating current evolution that is more rapid than will be experienced in practise. If the plasma resistivity is, in general, lower during this phase than assumed from neoclassical resistivity calculations it implies the possibility that flux consumption of future devices modelled in this way will actually be lower than calculated during this phase. This suggests that the overall performance of future devices could be better than that predicted on

the basis of diffusive models of current evolution employing neoclassical resistivity.

Acknowledgment

This work has been carried out within the framework of the EUROfusion Consortium and has received funding from the Euratom research and training programme 2014–2018 under grant agreement No 633053 and from the RCUK Energy Programme (Grant number EP/P012450/1). To obtain further information on the data and models underlying this paper please contact PublicationsManager@ccfe.ac.uk. The views and opinions expressed herein do not necessarily reflect those of the European Commission or the ITER Organisation.

References

- [1] Spitzer L. and Härm R. 1953 *Phys. Rev.* **89** 977–81
- [2] Hinton F.L. and Hazeltine R.D. 1976 *Rev. Mod. Phys.* **42** 239
- [3] Kikuchi M. and Azumi M. 1995 *Plasma Phys. Control. Fusion* **37** 1215–38
- [4] Hawryluk R.J., Bol K. and Johnson D. 1979 *Nucl. Fusion* **19** 1519
- [5] Meservey E. et al 1984 *Nucl. Fusion* **24** 3
- [6] Ejima S. et al 1982 *Nucl. Fusion* **22** 1627
- [7] Rohr H., Steuer K.H. and the ASDEX Team 1988 *Rev. Sci. Instrum.* **59** 1875
- [8] Becker G. 1989 *Nucl. Fusion* **29** 1291
- [9] Alladio F. et al 1993 Density limit and confinement in FTU ohmic plasma *Proc. 14th Conf. on Plasma Physics and Controlled Nuclear Fusion Research (Wurzburg, 30 September–7 October 1992)* vol 1 (Vienna: IAEA) p 141 (www-naweb.iaea.org/naweb/physics/FEC/STIPUB906_VOLI.pdf)
- [10] Greenwald M. et al 1995 *Phys. Plasmas* **2** 2308
- [11] Toi K. et al 1979 *Nucl. Fusion* **19** 1643
- [12] Challis C.D. et al 1989 *Nucl. Fusion* **29** 563
- [13] Bartlett D.V. et al 1988 *Nucl. Fusion* **28** 73
- [14] Kikuchi M. et al 1990 *Nucl. Fusion* **30** 343
- [15] Zarnstorff M.C. et al 1990 *Phys. Fluids B* **2** 1852
- [16] Joffrin E., Basiuk V., Bregeon R. and Litaudon X. 2000 *Plasma Phys. Control. Fusion* **42** 1227
- [17] McCormick K. 1986 Measurement of the poloidal Field Distribution in a Tokamak Plasma via Neutral Lithium Beam Spectroscopy *Proc. Conf. and Workshop on: Basic and Advanced Diagnostic Techniques for Fusion Plasmas (Varenna, 3–13 September 1986)* vol II (<https://publications.europa.eu/en/publication-detail/-/publication/05d55fd3-974c-42ad-bb30-01e0311cc4cd>) p 635
- [18] Levinton F.M. et al 1989 *Phys. Rev. Lett.* **63** 2060
- [19] McCormick K. et al 1987 *Phys. Rev. Lett.* **58** 491
- [20] Wootton A.J. 1988 Turbulence, transport and q measurements in TEXT *Proc. 12th Int. Conf. on Plasma Physics and Controlled Nuclear Fusion Research (Nice, 12–19 October 1988)* vol 1 (Vienna: IAEA) p 293 (www-naweb.iaea.org/naweb/physics/FEC/STIPUB787_VOLI.pdf)
- [21] Kaye S.M. et al 1992 *Phys. Fluids B* **4** 651
- [22] Rice B.W. 1992 *Rev. Sci. Instrum.* **63** 5002
- [23] Brower D.L., Zeng L. and Jiang Y. 1997 *Rev. Sci. Instrum.* **68** 419
- [24] Forest C.B. et al 1994 *Phys. Rev. Lett.* **73** 2444
- [25] Batha S.H. et al 1997 *Phys. Plasmas* **4** 3614
- [26] Kelliher D.J., Hawkes N.C. and McCarthy P.J. 2005 *Plasma Phys. Control. Fusion* **47** 1459
- [27] Gruber O. et al 1999 *Phys. Rev. Lett.* **83** 1787
- [28] Luce T.C. et al 2003 *Nucl. Fusion* **43** 321
- [29] Oyama N. et al 2009 *Nucl. Fusion* **49** 065026
- [30] Casper T.A. et al 2007 *Nucl. Fusion* **47** 825
- [31] Takizuka T. 2014 *Nucl. Fusion* **54** 092001
- [32] Na Y.-S. et al 2006 *Nucl. Fusion* **46** 232
- [33] Jenkins I. 2011 *Proc. of the 37th EPS Conf. on Plasma Physics (Dublin, Ireland, 21–25 June 2010)* p P1.104 (<http://ocs.ciemat.es/EPS2010PAP/pdf/P2.178.pdf>)
- [34] Keeling D. et al 2011 38th EPS Conf. on Plasma Physics (Strasbourg, 27 June–1 July 2011) (<http://ocs.ciemat.es/eps2011pap/pdf/O5.130.pdf>)
- [35] Citrin J. et al 2012 *Plasma Phys. Control. Fusion* **54** 065008
- [36] Voitikhovitch I. et al 2010 *Plasma Phys. Control. Fusion* **52** 105011
- [37] Garcia J. et al 2011 *Nucl. Fusion* **51** 073019
- [38] Lao L.L., St John H., Stambaugh R.D. and Pfeiffer W. 1985 *Nucl. Fusion* **10** 1421
- [39] Barbato E. et al 2014 *Nucl. Fusion* **54** 123009
- [40] Garcia J. 2013 *Plasma Phys. Control. Fusion* **55** 085006
- [41] Nunes I. et al 2014 *Proc. 25th IAEA Fusion Energy Conf. (St. Petersburg, October 13–18 2014)* (www-naweb.iaea.org/naweb/physics/FEC/FEC2014/fec2014-preprints/187_EX92.pdf)
- [42] Hobirk J. et al 2012 *Plasma Phys. Control. Fusion* **54** 095001
- [43] Goldston R.J., McCune D.C. and Towner H.H. 1981 *J. Comput. Phys.* **43** 61
- [44] Houlberg W.A. 1997 *Phys. Plasmas* **4** 3230
- [45] Sauter O., Angioni C. and Lin-Liu Y.R. 1999 *Phys. Plasmas* **6** 2834
- [46] Sauter O., Angioni C. and Lin-Liu Y.R. 2002 *Phys. Plasmas* **9** 5140
- [47] Lloyd B. et al 2004 *Plasma Phys. Control. Fusion* **46** B477
- [48] Belli E.A. and Candy J. 2012 *Plasma Phys. Control. Fusion* **54** 015015
- [49] Mikkelsen D.R. 1989 *Phys. Fluids B* **1** 333
- [50] Morris A.W. 2012 *IEEE Trans. Plasma Sci.* **40** 682
- [51] Homfray D.A. et al 2009 23rd IEEE/NPSS Symp. on Fusion Engineering (San Diego, USA, 1–5 June 2009) (<http://ieeexplore.ieee.org/document/5226423/>)
- [52] Dreicer H. 1959 *Phys. Rev.* **115** 238